



Validation of XCH₄ derived from SWIR spectra of GOSAT TANSO-FTS with aircraft measurement data

M. Inoue¹, I. Morino¹, O. Uchino¹, Y. Miyamoto², T. Saeki^{1,*}, Y. Yoshida¹, T. Yokota¹, C. Sweeney³, P. P. Tans³, S. C. Biraud⁴, T. Machida¹, J. V. Pittman⁵, E. A. Kort^{6,**}, T. Tanaka^{1,***}, S. Kawakami⁷, Y. Sawa⁸, K. Tsuboi⁸, and H. Matsueda⁸

¹National Institute for Environmental Studies (NIES), Tsukuba, Japan

²Graduate School of Natural Science and Technology, Okayama University, Okayama, Japan

³National Oceanic and Atmospheric Administration (NOAA), Boulder, CO, USA

⁴Lawrence Berkeley National Laboratory (LBNL), Berkeley, CA, USA

⁵Department of Earth and Planetary Sciences, Harvard University, Cambridge, MA, USA

⁶Jet Propulsion Laboratory/California Institute of Technology, Pasadena, CA, USA

⁷Japan Aerospace Exploration Agency (JAXA), Tsukuba, Japan

⁸Meteorological Research Institute (MRI), Tsukuba, Japan

* now at: Japan Agency for Marine-Earth Science and Technology (JAMSTEC), Yokohama, Japan

** now at: Department of Atmospheric, Oceanic and Space Sciences, University of Michigan, Ann Arbor, MI, USA

*** now at: NASA Ames Research Center, Moffett Field, CA, USA

Correspondence to: M. Inoue (inoue.makoto@nies.go.jp)

Received: 25 March 2014 – Published in Atmos. Meas. Tech. Discuss.: 9 May 2014

Revised: 12 August 2014 – Accepted: 12 August 2014 – Published: 17 September 2014

Abstract. Column-averaged dry-air mole fractions of methane (XCH₄), retrieved from Greenhouse gases Observing SATellite (GOSAT) short-wavelength infrared (SWIR) spectra, were validated by using aircraft measurement data from the National Oceanic and Atmospheric Administration (NOAA), the US Department of Energy (DOE), the National Institute for Environmental Studies (NIES), the HIAPER Pole-to-Pole Observations (HIPPO) program, and the GOSAT validation aircraft observation campaign over Japan. In the calculation of XCH₄ from aircraft measurements (aircraft-based XCH₄), other satellite data were used for the CH₄ profiles above the tropopause. We proposed a data-screening scheme for aircraft-based XCH₄ for reliable validation of GOSAT XCH₄. Further, we examined the impact of GOSAT SWIR column averaging kernels (CAK) on the aircraft-based XCH₄ calculation and found that the difference between aircraft-based XCH₄ with and without the application of the GOSAT CAK was less than ±9 ppb at maximum, with an average difference of −0.5 ppb.

We compared GOSAT XCH₄ Ver. 02.00 data retrieved within ±2° or ±5° latitude-longitude boxes centered at each aircraft measurement site with aircraft-based XCH₄ measured on a GOSAT overpass day. In general, GOSAT XCH₄ was in good agreement with aircraft-based XCH₄. However, over land, the GOSAT data showed a positive bias of 1.5 ppb (2.0 ppb) with a standard deviation of 14.9 ppb (16.0 ppb) within the ±2° (±5°) boxes, and over ocean, the average bias was 4.1 ppb (6.5 ppb) with a standard deviation of 9.4 ppb (8.8 ppb) within the ±2° (±5°) boxes. In addition, we obtained similar results when we used an aircraft-based XCH₄ time series obtained by curve fitting with temporal interpolation for comparison with GOSAT data.

1 Introduction

It is well known that atmospheric methane (CH₄) is an important greenhouse gas (GHG) that plays a crucial role in global climate change and atmospheric chemistry. CH₄

concentrations have been measured from various in situ platforms, including ground-based stations, tall towers, ships, aircraft, and balloons (e.g., Cavanagh et al., 1969; Fraser et al., 1981; Steele et al., 1987; Blake and Rowland, 1988; Aoki et al., 1992; Dlugokencky et al., 1994; Matsueda and Inoue, 1996; Tohjima et al., 1997, 2002; Andrews et al., 2001; Sasakawa et al., 2010; Terao et al., 2011; Wada et al., 2011). Although these measurements have provided extensive information on the spatial and temporal variations of atmospheric CH₄, the distribution of the CH₄ sources and sinks is still poorly understood because of the sparseness of available in situ observations and their limited altitudinal range.

By using satellite observations, it should be possible to determine the global distribution of CH₄ and, in conjunction with atmospheric inverse modeling, to estimate its sources and sinks with improved accuracy at the subcontinental scale (e.g., Bergamaschi et al., 2007, 2009; Meirink et al., 2008; Fraser et al., 2013). Vertical CH₄ profiles have been retrieved from thermal infrared (TIR) spectra obtained with satellite-borne instruments, including the Interferometric Monitor for Greenhouse gases (IMG; Clerbaux et al., 2003), the Atmospheric Infrared Sounder (AIRS; Aumann et al., 2003), the Infrared Atmospheric Sounding Interferometer (IASI; Crevoisier et al., 2009), and the Tropospheric Emission Spectrometer (TES; Wecht et al., 2012). In addition, near-infrared (NIR) spectra obtained by the SCanning Imaging Absorption spectroMeter for Atmospheric CHartographY (SCIAMACHY) onboard Envisat, launched in March 2002, provide column-averaged dry-air mole fractions of CH₄ (XCH₄), which have been compared to ground-based Fourier transform spectrometer (FTS) measurements and model results (e.g., Dils et al., 2006; Schneising et al., 2009, 2012).

The Greenhouse gases Observing SATellite (GOSAT), the world's first satellite specialized for measuring the concentrations of atmospheric carbon dioxide (CO₂) and CH₄ from space, was launched in January 2009 (Yokota et al., 2009). Observation results include column-averaged dry-air mole fractions of CO₂ (XCO₂) and XCH₄ retrieved from the short-wavelength infrared (SWIR) spectra of the Thermal And Near-infrared Sensor for carbon Observation (TANSO)-FTS onboard GOSAT (Yoshida et al., 2011, 2013; Morino et al., 2011; Parker et al., 2011; Schepers et al., 2012). Yoshida et al. (2013) evaluated the mean bias of GOSAT SWIR XCH₄ (Ver. 02.00, June 2009 to July 2010) to be -6.1 ppb with a standard deviation of 12.3 ppb by using data from the Total Carbon Column Observing Network (TCCON), a worldwide network of ground-based FTSs (Wunch et al., 2010, 2011). Gavrilov et al. (2014) also compared GOSAT XCH₄ data with ground-based FTS data obtained near St. Petersburg, Russia (see Sect. 3.3.3 for details).

Along with ground-based FTS data, aircraft measurements are also useful for validation of GOSAT data. However, only a few studies have compared satellite-retrieved XCO₂ or XCH₄ data with aircraft measurements. Saitoh et al. (2012) compared GOSAT SWIR XCH₄ Ver. 01.xx data (i.e., the

previous version) and XCH₄ calculated from TIR CH₄ profiles with aircraft measurement data obtained over Guam in the North Pacific Ocean by the Comprehensive Observation Network for TRace gases by AIRLiner (CONTRAIL) project (Machida et al., 2008). In addition, our previous study (Inoue et al., 2013) validated GOSAT SWIR XCO₂ data with aircraft measurement data from ~ 40 sites.

In this study, we validated GOSAT SWIR XCH₄ Ver. 02.00 data by using various vertical measurement data obtained by aircraft. We used the same two approaches that Inoue et al. (2013) used for XCO₂ validation: the first approach uses spatiotemporally matched data, and the second uses spatially matched but temporally interpolated data obtained by curve fitting. In Sect. 2, we describe the data used in this study and the method used to calculate XCH₄ from the aircraft-measured profile data. In Sect. 3, we examine how the use of GOSAT SWIR column averaging kernels (CAK) and the vertical coverage of aircraft measurements affect the aircraft-based XCH₄ calculations. Thereafter, we show the validation results from the two approaches described above. In Sect. 4, we summarize our findings and present our conclusions.

2 Data and analysis methods

2.1 XCH₄ retrieved from GOSAT TANSO-FTS SWIR spectra

GOSAT was launched on 23 January 2009 into a Sun-synchronous orbit to monitor the distributions of GHGs (Kuze et al., 2009). GOSAT crosses the Equator at about 13:00 LT and returns to the same point in space every 3 days, during which the TANSO-FTS makes observations of several tens of thousands of ground points globally. TANSO-FTS has three bands in the SWIR region, centered at 0.76, 1.6, and $2.0\text{ }\mu\text{m}$, and a broad TIR band between 5.6 and $14.3\text{ }\mu\text{m}$. Measurements in the SWIR and TIR bands allow for the retrieval of XCH₄ and CH₄ concentration profiles, respectively, in cloud-free regions (Yoshida et al., 2011, 2013; Saitoh et al., 2012). In this study, we used aircraft measurement data to validate SWIR Ver. 02.00 XCH₄ data retrieved with the latest retrieval algorithm (Yoshida et al., 2013), which covers the period from June 2009 to July 2010.

2.2 XCH₄ calculation from aircraft measurement data

2.2.1 Aircraft measurements

The NOAA Earth System Research Laboratory (ESRL) Global Monitoring Division measures CH₄ concentrations over North America and the Pacific Ocean from aircraft (e.g., Xiong et al., 2008). Air samples are routinely collected in flasks at about 20 sites, covering an altitude range of ~ 0.5 to 7 km with vertical resolutions of 0.3 – 0.7 km , at weekly or

biweekly sampling intervals. The reported analytical uncertainty of the CH₄ concentration is ~ 2 ppb.

The US Department of Energy (DOE) supports an aircraft-based observation program over the Southern Great Plains (SGP; see Table 1 for all site codes) as part of a joint effort between the Atmospheric Radiation Measurement (ARM) program, NOAA/ESRL, and the Lawrence Berkeley National Laboratory ARM Carbon project (Biraud et al., 2013). Flasks of air samples are collected about twice weekly by small aircraft (initially a Cessna 172, currently a Cessna 206) during a series of horizontal legs ranging in altitude from 0.46 to 5.5 km and analyzed by NOAA/ESRL for a suite of GHGs and isotopes, thereby linking all flights to the global cooperative air-sampling network.

Over three sites in Siberia and Sagami Bay, Japan, aircraft sampling is conducted by the National Institute for Environmental Studies (NIES) once or twice a month. Typical observing altitudes are 0.5–7 km with vertical resolutions of 0.5–1.5 km (Machida et al., 2001). CH₄ mixing ratios of the flask samples are measured with a precision of about 2 ppb by using a gas chromatograph equipped with a flame ionization detector (Machida et al., 2008). The standard gases used for flask measurement were calibrated against NIES 94 CH₄ scale, which was higher than NOAA 04 scale by 3.5–4.6 ppb in the range between 1750 and 1840 ppb (Terao et al., 2011).

Aircraft measurements obtained by the HIAPER Pole-to-Pole Observations (HIPPO) project are also available for GOSAT validation. The HIPPO project consisted of five global aircraft measurement missions, covering the different seasons, during which the atmosphere was sampled and measured from the North Pole to the coastal waters of Antarctica in the Pacific Basin (Wofsy et al., 2011). Most HIPPO profiles extend from altitudes of approximately 0.3 to 8.5 km, but some extend to above 14 km. HIPPO flights measured high CH₄ concentrations near the surface over the Arctic Ocean (Kort et al., 2012), a finding that suggests that surface waters of the Arctic Ocean may be an important source of CH₄. Here, we utilized 10 s merged CH₄ profiles based on quantum cascade laser system (QCLS) measurements obtained during the second and third HIPPO missions (HIPPO-2 and HIPPO-3), which took place from October to November 2009 and from March to April 2010, respectively (Wofsy et al., 2012). The QCLS observations and NOAA flask sample results (QCLS CH₄ minus NOAA flask CH₄) differed by 3.9 ppb (HIPPO-2) and 6.0 ppb (HIPPO-3). Therefore, we subtracted the respective value from the QCLS data obtained by each mission to improve consistency of the HIPPO data with global NOAA network data (i.e., in this study, QCLS data calibrated against NOAA flask data were used).

In addition, aircraft measurements are conducted over Japan by NIES and the Japan Aerospace Exploration Agency (JAXA) once or twice a year (hereinafter NIES-JAXA campaign) to calibrate the ground-based FTS data utilized for GOSAT validation as well as for direct validation of GOSAT data. In this study, we used CH₄ concentrations with an

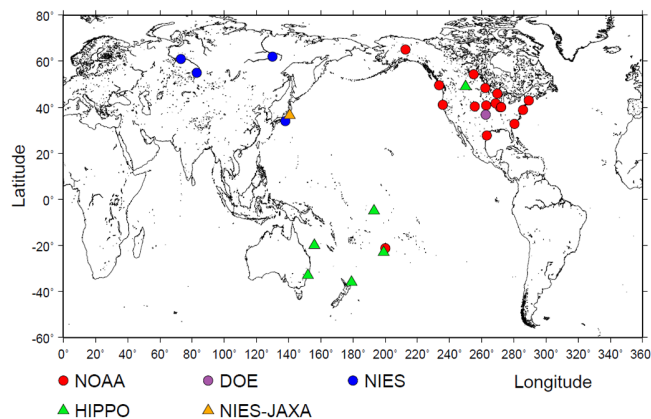


Figure 1. Global distribution of the aircraft measurement sites used for GOSAT validation.

analytical precision of better than 1.7 ppb obtained by flask sampling over Tsukuba (36.1° N, 140.1° E) in February 2010 (Tanaka et al., 2012). Because airspace controls at two international airports restricted flights over Tsukuba to altitudes below about 2 km (Tanaka et al., 2012), samples from altitudes between 2 and 7 km were obtained over Kumagaya, about 70 km west of Tsukuba. In addition, measurements made at 1.5, 25, 100, and 200 m a.g.l. on a tall tower of the Meteorological Research Institute (MRI) in Tsukuba (36.1° N, 140.1° E; Inoue and Matsueda, 1996, 2001) provide information about CH₄ concentrations below the lower boundary of the aircraft measurements. Thus, in this study, we used CH₄ profiles measured over Kumagaya along with aircraft and tower measurements over Tsukuba for the calculation of XCH₄ over Tsukuba.

As noted above, the HIPPO missions were able to provide atmospheric measurements covering altitudes from 0.3 km up to 14 km. On the other hand, typical observing altitudes of the NOAA, DOE, NIES, and NIES-JAXA campaign were from 0.5 km up to about 6 or 7 km. Altogether, we used CH₄ profiles obtained at 16 NOAA sites, 1 DOE site, and 4 NIES sites, as well as on 2 HIPPO missions and during 1 NIES-JAXA campaign, for validation of GOSAT SWIR XCH₄ data (Fig. 1 and Table 1).

2.2.2 Tropospheric profiles and tropopause height

Because the aircraft measurements were made with a limited altitude range, we needed additional observations from near the ground and above the tropopause. For these observations, we made certain assumptions. We reconstructed CH₄ profiles in the troposphere in a manner analogous to the aircraft-based XCO₂ calculations made by Araki et al. (2010). First, we extrapolated the lowest aircraft data to the surface. Then, for aircraft profiles where all observations were below the tropopause, we assumed that the CH₄ concentration remained constant from that measured at highest observational altitude up to the tropopause. Next, we

Table 1. Basic information on the aircraft observation sites.

(a) NOAA					
Site code	Latitude [deg. N]	Longitude [deg. E]	Elevation [m]	Region	Site name
PFA	65.1	-147.3	210	United States	Poker Flat, Alaska
BRM	54.3	-105.0	507	Canada	BERMS, Saskatchewan
ESP	49.6	-126.4	7	Canada	Estevan Point, British Columbia
DND	48.4	-97.8	464	United States	Dahlen, North Dakota
LEF	45.9	-90.3	472	United States	Park Falls, Wisconsin
NHA	43.0	-70.6	0	United States	Worcester, Massachusetts
WBI	41.7	-91.4	242	United States	West Branch, Iowa
THD	41.1	-124.2	107	United States	Trinidad Head, California
BNE	40.8	-97.2	466	United States	Beaver Crossing, Nebraska
CAR	40.4	-104.3	1740	United States	Briggsdale, Colorado
HIL	40.1	-87.9	202	United States	Homer, Illinois
AAO	40.1	-88.6	213	United States	Airborne Aerosol Observing, Illinois
CMA	38.8	-74.3	0	United States	Cape May, New Jersey
SCA	32.8	-79.6	0	United States	Charleston, South Carolina
TGC	27.7	-96.9	0	United States	Sinton, Texas
RTA	-21.3	-159.8	3	Cook Islands	Rarotonga

(b) DOE					
SGP	36.8	-97.5	314	United States	Southern Great Plains, Oklahoma

(c) NIES					
YAK	62	130	136	Russia	Yakutsk
SUR	61	73	35	Russia	Surgut
NOV	55	83	143	Russia	Novosibirsk
SGM	35.1	139.3	0	Japan	Sagami Bay

(d) HIPPO					
HPA	49	-110	1040	United States	northeastern part of Great Falls, Montana
HPB	-23	-161	0	South Pacific Ocean	southwestern part of Rarotonga
HPC	-33	152	0	Australia	east coast of Newcastle
HPD	-20	156	0	Coral Sea	western part of Chesterfield Islands
HPE	-5	-167	0	Kiribati	western part of Enderbury
HPF	-36	179	0	New Zealand	northeastern part of Bay of Plenty

(e) NIES-JAXA campaign					
TKB	36.1	140.1	31	Japan	Tsukuba

drew a straight line connecting the CH₄ concentration at the tropopause with the lowest satellite-based climatological value above the tropopause (see Sect. 2.2.3). The local tropopause height was derived by using the Global Forecast System model (<http://nomads.ncdc.noaa.gov/>) of the National Centers for Environmental Prediction (NCEP), the results of which agree well with radiosonde measurements (Pan and Munchak, 2011). We used Global Forecast System tropopause height data supplied as reanalysis values at 00:00, 06:00, 12:00, and 18:00 UTC and the forecast values at 03:00, 09:00, 15:00, and 21:00 UTC (3 h after each reanalysis time) on 1° × 1° horizontal grids. In the few cases that aircraft measurements were made above the tropopause, a

straight line was drawn connecting the aircraft data obtained at the highest measurement altitude with the satellite-based climatological data obtained above that altitude.

2.2.3 Stratospheric and mesospheric profiles

The Atmospheric Chemistry Experiment (ACE)-FTS aboard the Canadian satellite SCISAT, launched in August 2003, was designed to clarify vertical structures of over 30 chemical species, including CH₄, in the upper troposphere, stratosphere, and mesosphere by means of the solar occultation technique (Bernath et al., 2005). We used ACE-FTS zonal mean climatological data (<http://www.ace.uwaterloo.ca/>) as the currently most probable data to complete the

stratospheric and mesospheric parts of CH₄ profiles, averaged on a monthly basis over the period from February 2004 to February 2009, at 5° latitude spacing and 28 pressure levels from 300 to 0.1 hPa (Jones et al., 2012). The observing period of ACE-FTS data is relatively close to that of GOSAT data. The difference between ACE-FTS CH₄ concentrations and balloon-borne observations is less than 10 % between 15 and 24 km (De Mazière et al., 2008). At certain latitudes, ACE-FTS climatological data are not available for all months, owing to the character of the SCISAT orbit. Therefore, we utilized climatological data based on measurements made by the Halogen Occultation Experiment (HALOE) onboard the Upper Atmosphere Research Satellite (UARS), launched in September 1991, for months when ACE-FTS climatological data were unavailable. The monthly HALOE climatological product (<http://www.atmos-chem-phys.net/5/2797/2005/acp-5-2797-2005-supplement.tar>), based on HALOE profiles between October 1991 and August 2002, is compiled for several gases, including CH₄, at 5° latitude spacing and 22 pressure levels between 316 and 0.1 hPa (Groß and Russell, 2005). HALOE CH₄ data and data from space shuttle flights, balloon-borne observations, and so on generally agree within 15 % (Park et al., 1996).

De Mazière et al. (2008), however, showed that CH₄ concentrations observed by HALOE show a negative bias compared with ACE-FTS data, with large differences above 35 km. This bias is attributed to the different observation period and the increase of the atmospheric CH₄ concentration between the observation periods. Figure 2 shows the percent differences of ACE-FTS and HALOE (ACE-FTS minus HALOE) relative to the average of the two instruments. We found that, below the altitude of 40 km, HALOE CH₄ concentrations were on average about 5 % lower (standard deviation, SD = ~ 15 %) than ACE-FTS concentrations, and from 40 to 65 km, they were 10–15 % lower (SD = ~ 20 %), consistent with the results of De Mazière et al. (2008). We used CH₄ profiles based on ACE-FTS data for months when ACE-FTS climatological data were available. In latitudinal bands where there were no ACE-FTS profiles for certain months, we used HALOE CH₄ concentration data adjusted by a scaling factor (blue dots in Fig. 2) (i.e., HALOE climatological profiles corrected by ACE-FTS data). In this study, we did not use the ACE or HALOE climatological data from below the tropopause or the maximum height of aircraft measurement for constructing CH₄ profiles (Sect. 2.2.2).

2.2.4 Dry-air number density profiles

To calculate aircraft-based XCH₄, we need to know the number density profile of dry air. We used meteorological data from the Committee on Space Research (COSPAR) International Reference Atmosphere (CIRA-86; Fleming et al., 1990), which provides empirical models of atmospheric temperature and densities from the surface to 120 km.

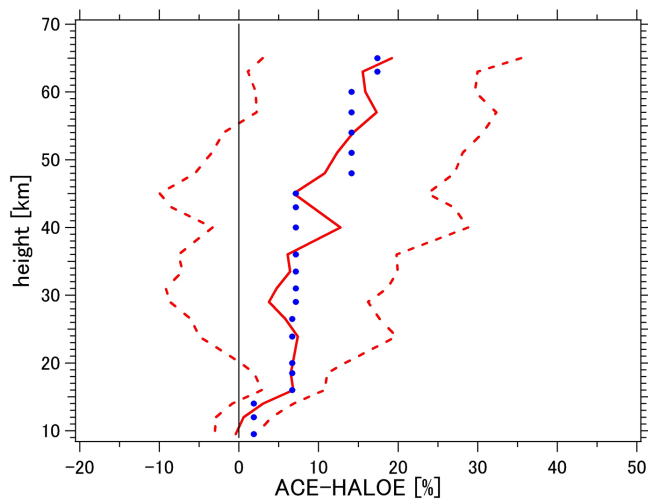


Figure 2. Average (solid red line) CH₄ concentration difference ± 1 SD (dashed red lines) between ACE-FTS and HALOE data. At latitudes without ACE-FTS profile data, the values shown by the blue dots at the respective altitudes were used instead of ACE-FTS CH₄ data for estimating stratospheric and mesospheric profiles. See text for more detail.

We here compared aircraft-based XCH₄ data calculated using only CIRA-86 data (without applying CAK; see Sect. 2.2.5) with XCH₄ calculated using the grid point value (GPV) data set prepared by the Japan Meteorological Agency (see Inoue et al., 2013). Because the upper boundary of the GPV data was 10 hPa, we used CIRA-86 data above the 10 hPa level (above ~ 30 km) to calculate XCH₄ in this comparison. In other words, we compared aircraft-based XCH₄ calculated by using GPV air number densities below the 10 hPa level and CIRA-86 densities above the 10 hPa level (GPV+CIRA XCH₄) with XCH₄ estimated by using vertical CIRA-86 profiles throughout the atmosphere (CIRA XCH₄). The average ± 1 SD of the difference between CIRA XCH₄ and GPV+CIRA XCH₄ over Park Falls (LEF) and SGP in 2009 were only 0.1 ± 1.4 ppb ($n = 22$) and 0.2 ± 1.0 ppb ($n = 46$), respectively. Therefore, we calculated XCH₄ by using only CIRA-86 data for the dry-air number densities in this study.

2.2.5 Aircraft-based CH₄ profiles and calculation of XCH₄ with and without applying GOSAT column averaging kernels (CAK)

Figure 3 shows an example of aircraft-based CH₄ profiles obtained over Charleston, South Carolina (SCA), USA. The vertical coordinate is represented by geometric height (left axis) and pressure (right axis). Following the method used by Inoue et al. (2013) for XCO₂, we calculated XCH₄ from the reconstructed CH₄ profiles with and without applying the GOSAT CAK.

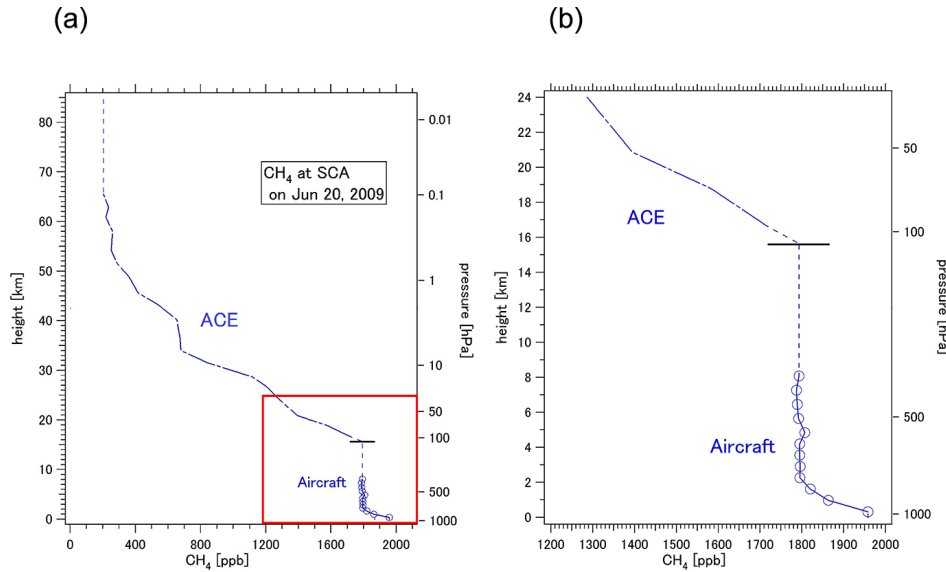


Figure 3. An example of CH₄ profiles constructed over Charleston, South Carolina (SCA), USA. **(a)** High-altitude profile. The red rectangular area is expanded in **(b)**. Vertical coordinate is represented by geometric height (left axis) and pressure (right axis). The blue circles represent aircraft measurements and are connected by solid lines. The horizontal black lines indicate the tropopause. The dash-dotted lines represent the profile above the tropopause based on the ACE-FTS or HALOE climatology (ACE-FTS in this case), and the dashed lines show the part of the CH₄ profile that was assumed. See Sects. 2.2.2. and 2.2.3 for more detail.

CAK \mathbf{a} is expressed as follows:

$$\mathbf{a}_j = (\mathbf{h}^T \mathbf{A})_j \frac{1}{\mathbf{h}_j}, \quad (1)$$

where \mathbf{A} and \mathbf{h} denote the averaging kernel matrix and a pressure-weighting function calculated on the basis of the dry-air number density profile, respectively. The subscript j is the index of the j th layer. Thus, the XCH₄ values derived from the aircraft profile weighted by the CH₄ CAK \mathbf{a} are calculated as follows:

$$\begin{aligned} X_{\text{CH}_4}^{\text{in situ,CAK}} &= X_{\text{CH}_4}^{\text{a}} + \sum_j \mathbf{h}_j \mathbf{a}_j (t_{\text{in situ}} - t_a)_j \\ &= \mathbf{h}^T [\mathbf{A} \cdot t_{\text{in situ}} + (\mathbf{I} - \mathbf{A}) t_a], \end{aligned} \quad (2)$$

where $X_{\text{CH}_4}^{\text{a}}$ is the column-averaged dry-air mole fraction of CH₄ in the a priori profile t_a , and $t_{\text{in situ}}$ is the aircraft-based CH₄ profile. The a priori CH₄ profile of GOSAT is calculated for every observation day by an offline tracer transport model developed by NIES (NIES TM; Maksyutov et al., 2008; Saeki et al., 2013).

Aircraft-based XCH₄ values can be calculated without applying the CH₄ CAK as follows:

$$X_{\text{CH}_4}^{\text{in situ,noCAK}} = \mathbf{h}^T \cdot t_{\text{in situ}}. \quad (3)$$

We integrated Eqs. (2) and (3) over altitudes from the surface up to 85 km with a vertical resolution of 100 m based on the method used by Araki et al. (2010) for XCO₂. As described below (Sect. 2.2.6), our aim was to validate GOSAT

XCH₄ by using only aircraft-based XCH₄ data with an uncertainty of less than 1 standard deviation at each respective site.

2.2.6 Uncertainty of aircraft-based XCH₄ and data screening

It is important for the data used to validate GOSAT SWIR XCH₄ to be as reliable as possible. To screen out aircraft-based XCH₄ outliers, we defined and evaluated the “total uncertainty” for each aircraft site, except for the HIPPO and NIES-JAXA campaign sites, where there were few data from the same locations. To calculate the total uncertainty, we first divided the atmospheric layer from the surface to the mesopause (85 km) into three domains: (I) below the planetary boundary layer (PBL), (II) from the PBL to the tropopause, and (III) above the tropopause. We then attempted to fit Eq. (4), below, to partial XCH₄ values in each domain based on the method used by Miyamoto et al. (2013) and Inoue et al. (2013) for XCO₂:

$$\begin{aligned} \text{XCH}_4(t) &= \text{Intercept} + \text{Trend} \times t + \frac{\text{Amp}_1}{2} \\ &\times \cos\left(2\pi \frac{t - \Phi_1}{12}\right) + \frac{\text{Amp}_2}{2} \times \cos\left(4\pi \frac{t - \Phi_2}{12}\right), \end{aligned} \quad (4)$$

where XCH₄(t) is the partial XCH₄ value at time t [month], Intercept represents the partial XCH₄ on 1 January 2007 without sinusoidal variations, and Trend denotes the monthly growth rate. Amp₁ and Amp₂ are the amplitudes of sinusoidal variations with periods of 12 and 6 months,

Table 2. Uncertainties of partial XCH₄ at each aircraft observation site for domain I, below the planetary layer (PBL) (σ_{pbl}); II, from the PBL to the tropopause (σ_{trp}); and III, above the tropopause (σ_{str}). In addition, σ_{pbl} when there were aircraft data for the PBL and when there were no aircraft data for the PBL ($\sigma_{\text{pbl_withdata}}$ and $\sigma_{\text{pbl_nodata}}$) were also evaluated separately. The numbers shown in parentheses indicate that the number of measurements used to determine $\sigma_{\text{pbl_nodata}}$ was less than seven. See text for details.

Site	Number of measurements	σ_{pbl} [ppb]	σ_{trp} [ppb]	σ_{str} [ppb]	Number (with data in PBL)	$\sigma_{\text{pbl_withdata}}$ [ppb]	Number (without data in PBL)	$\sigma_{\text{pbl_nodata}}$ [ppb]
PFA	105	14.0	10.1	44.3	42	14.5	63	12.8
BRM	87	24.6	12.1	42.3	37	11.7	50	29.8
ESP	148	10.8	12.3	53.8	109	11.0	39	9.0
DND	53	25.0	12.0	58.6	32	16.7	21	29.5
LEF	126	23.0	11.5	49.5	84	17.9	42	27.4
NHA	117	24.2	11.3	47.0	83	20.5	34	27.3
WBI	76	19.1	10.0	42.1	51	16.0	25	21.7
THD	61	25.3	12.7	50.7	42	16.7	19	33.3
BNE	67	34.7	10.3	38.7	31	30.6	36	33.2
CAR	114	18.7	12.9	49.7	9	11.7	105	18.3
HIL	83	22.6	11.7	55.9	49	19.0	34	23.9
AAO	252	28.1	12.9	51.2	196	25.2	56	36.0
CMA	131	35.2	13.0	54.4	91	26.2	40	46.6
SCA	84	36.8	12.4	51.6	77	36.7	7	25.8
TGC	84	60.8	11.4	58.0	80	57.6	(4)	–
RTA	59	4.5	5.1	34.1	55	4.1	(4)	–
SGP	243	56.6	17.0	45.0	213	47.2	30	83.3
YAK	15	14.7	7.4	26.1	9	8.8	(6)	–
SUR	21	23.8	11.6	43.1	15	16.9	(6)	–
NOV	17	32.0	12.1	43.2	10	26.9	7	29.1
SGM	22	34.6	14.5	43.8	14	34.1	8	20.7
ALL	1965	32.7	12.5	48.7	1329	30.3	616	31.8

respectively, whereas Φ_1 and Φ_2 are phases of the annual and semianual sinusoidal variations, respectively. Figure 4 shows the temporal variations of the partial XCH₄ calculated in the three domains (I, II, and III) over SGP. The time series of partial XCH₄ were calculated from aircraft profiles or assumed profiles below the PBL height for domain I (Fig. 4a), from aircraft profiles between the PBL height and the tropopause for domain II (Fig. 4b), and from ACE/corrected HALOE data in the stratosphere and mesosphere for domain III (Fig. 4c). The trend of the partial XCH₄ from the PBL through the tropopause was about 0.3 ppb month⁻¹, and the fitting error caused by this constant trend was as small as 0.06 ppb month⁻¹. Obviously, the tropospheric CH₄ concentrations (Fig. 4a and b) are lower in summer and higher in cold seasons. This seasonality is due to CH₄ oxidation by OH radicals, which are more abundant in summer. The standard deviations of the differences between the partial XCH₄ values and the gap-filled data in domains I, II, and III were calculated and expressed as σ_{pbl} , σ_{trp} , and σ_{str} , respectively. Moreover, two categories of differences, $\sigma_{\text{pbl_withdata}}$ and $\sigma_{\text{pbl_nodata}}$, were also calculated in domain I depending on whether the lowest aircraft data were obtained in the PBL, provided that at least seven measurements were available in each category. Table 2 summarizes σ_{pbl} , $\sigma_{\text{pbl_withdata}}$, $\sigma_{\text{pbl_nodata}}$, σ_{trp} , and σ_{str} at all sites. For instance,

at SGP ($n = 243$), the uncertainties of the partial XCH₄ in domain I with data ($n = 213$), I without data ($n = 30$), II, and III were 47.2, 83.3, 17.0, and 45.0 ppb, respectively. Overall, the σ_{pbl} results showed prominent regional differences, from 4.5 ppb at Rarotonga, Cook Islands (RTA), to 60.8 ppb at Sinton, Texas (TGC). In domain II, the uncertainties of partial XCH₄ were only 10–15 ppb, the smallest uncertainties in all domains at most sites. In addition, we examined whether the uncertainties of the respective partial XCH₄ values were strongly seasonal at four sites (SGP, RTA, LEF, and SGM). Monthly time series of σ_{pbl} , σ_{trp} , and σ_{str} of the partial XCH₄ data at SGP, RTA, and LEF did not show a strong seasonal dependence (Fig. 5a, b, and c), and the uncertainties calculated for the entire period can be reasonably used as threshold values for data screening. On the other hand, it was difficult to investigate seasonality of the uncertainties at several sites such as SGM due to lack of data for all months (Fig. 5d). Using the uncertainties in each domain, we estimated the total uncertainty (σ_{total}) at each site, following the method used by Miyamoto et al. (2013) for XCO₂:

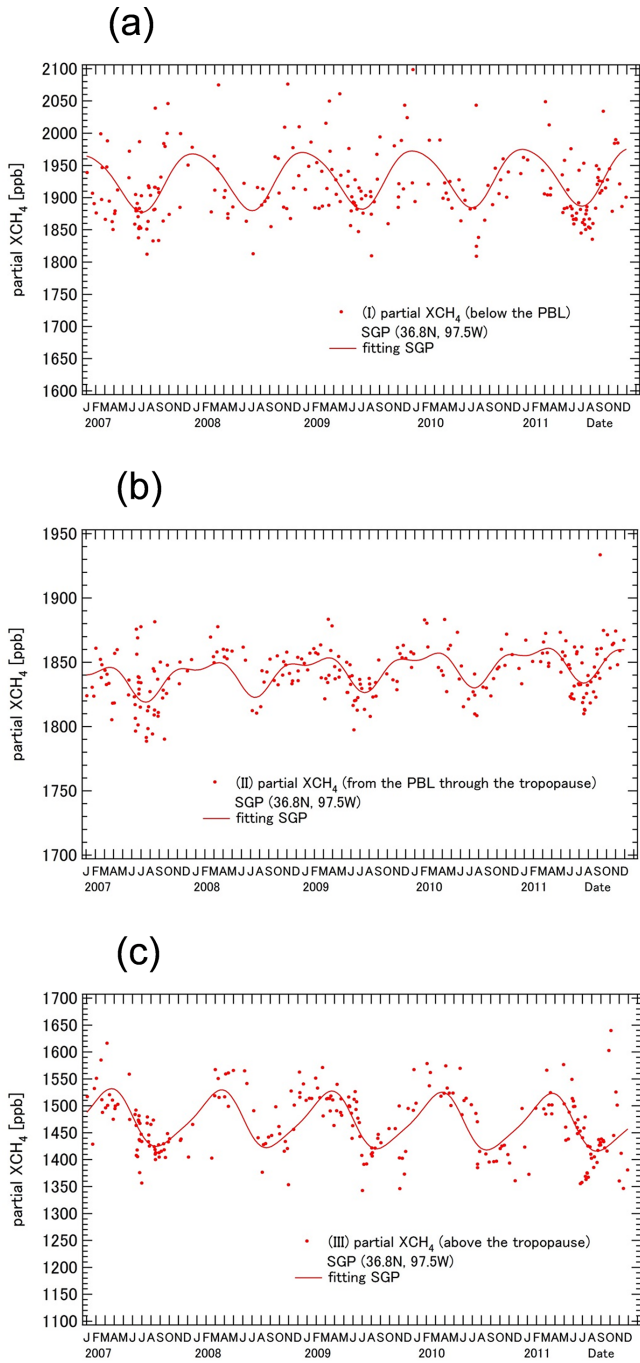


Figure 4. Temporal variations of partial XCH₄ over the Southern Great Plains (SGP), calculated (**a**) below the PBL (domain I), (**b**) from the PBL to the tropopause (domain II), and (**c**) above the tropopause (domain III). The dots represent partial XCH₄ data, and the lines are fitted curves. See text for more detail.

$$\sigma_{\text{total}} = \frac{\sqrt{\sum_j N(j)^2 \times \sigma(j)^2}}{N} \quad (j = \text{I, II, III})$$

$$= \frac{\sqrt{N_{\text{pbl}}^2 \times \sigma_{\text{pbl}}^2 + N_{\text{trp}}^2 \times \sigma_{\text{trp}}^2 + N_{\text{str}}^2 \times \sigma_{\text{str}}^2}}{N}, \quad (5)$$

where N_{pbl} , N_{trp} , and N_{str} are the partial dry-air number densities in domains I, II, and III, respectively, and N is the sum of N_{pbl} , N_{trp} , and N_{str} (i.e., $N = N_{\text{pbl}} + N_{\text{trp}} + N_{\text{str}}$). We used either $\sigma_{\text{pbl_withdata}}$ or $\sigma_{\text{pbl_nodata}}$ in Eq. (5) according to whether the lowest data were within the PBL to calculate σ_{total} . When the number of observations used to determine $\sigma_{\text{pbl_nodata}}$ was less than seven (denoted by a dash in Table 2), we used σ_{pbl} instead of $\sigma_{\text{pbl_nodata}}$. Table 3 summarizes the σ_{total} statistics for each observation site. We regarded aircraft-based XCH₄ data with σ_{total} larger than the sum of the average and 1 standard deviation of σ_{total} at each corresponding site as outlier data and screened them out. For example, the average plus 1 standard deviation of σ_{total} at SGP was 15.8 ppb plus 1.2 ppb. Therefore, we regarded their sum (17.0 ppb) as the threshold value at SGP for data screening, and removed aircraft-based XCH₄ data with σ_{total} larger than 17.0 ppb from all aircraft measurements obtained at SGP. At SGP, 4.9 % of all data were screened out, and the mean removal rate at all 21 sites was about 12 % (Table 3).

2.3 Methods for validating GOSAT products with aircraft data

We set the coincidence criteria between GOSAT and aircraft data as follows: GOSAT data retrieved within $\pm 2^\circ$ or $\pm 5^\circ$ latitude-longitude boxes centered at each observation site and aircraft-based XCH₄ on a GOSAT overpass day after outlier removal (described in Sect. 2.2.6) (i.e., extraction of temporally matched data for direct comparison). This means that the GOSAT data and aircraft measurement data were obtained on the same day at each site. When multiple aircraft data were associated with the particular GOSAT data, the aircraft data temporally nearest to the GOSAT overpass time were selected. The maximum time difference of matched data set was about 9 h. For this direct comparison, we used the aircraft-based XCH₄ with the application of CAK (Sect. 3.3.1).

This approach enabled us to validate GOSAT products with temporally matched observational data. However, no temporally matched data were available from several observation sites because no aircraft measurements were obtained on a GOSAT overpass day. Therefore, we also prepared temporally interpolated aircraft-based XCH₄ data by curve fitting for comparison with GOSAT XCH₄ (Sect. 3.3.2). In this case, we used the aircraft-based XCH₄ data for the curve fitting without applying GOSAT CAK, because when a curve-fitting approach is used, CAK cannot be applied to aircraft-based XCH₄ calculations in the absence of vertical

Table 3. Total uncertainty (σ_{total}) of aircraft-based XCH₄ and 1 standard deviation screening (data differing from the average by more than 1 standard deviation) at each aircraft observation site.

Site	Total uncertainty (σ_{total}) of XCH ₄			1 SD screening	
	Average [ppb]	SD [ppb]	Maximum [ppb]	Number screened out	Percentage screened out [%]
PFA	14.5	1.9	20.5	16	15.2
BRM	14.0	1.6	21.8	9	10.3
ESP	15.5	2.0	23.6	23	15.5
DND	16.4	2.3	22.8	7	13.2
LEF	14.6	2.3	23.0	21	16.7
NHA	13.6	2.0	22.3	14	12.0
WBI	11.7	1.9	21.2	10	13.2
THD	14.0	1.1	18.5	10	16.4
BNE	11.4	1.3	16.3	6	9.0
CAR	15.1	2.0	21.5	14	12.3
HIL	14.4	2.5	22.7	9	10.8
AAO	14.0	1.8	24.1	35	13.9
CMA	14.4	1.8	24.1	13	9.9
SCA	13.0	1.5	21.7	9	10.7
TGC	12.4	1.1	17.7	11	13.1
RTA	5.7	0.3	6.4	9	15.3
SGP	15.8	1.2	29.9	12	4.9
YAK	8.2	1.1	10.3	4	26.7
SUR	14.0	1.1	15.9	3	14.3
NOV	14.0	1.5	18.2	2	11.8
SGM	13.7	1.1	16.2	4	18.2
All data	—	—	—	241	12.3

information about all aircraft measurements (see Inoue et al., 2013, regarding XCO₂). We first evaluated the impact of CAK on the aircraft-based XCH₄ calculations to prevent misinterpretation of the validation results obtained by using the two different approaches (Sect. 3.1).

3 Results and discussion

3.1 Impact of GOSAT SWIR CAK application on aircraft-based XCH₄ calculations

We examined how aircraft-based XCH₄ values at each observation site differed when calculated with and without application of GOSAT SWIR CAK. The aircraft-based XCH₄ at a certain time of day was calculated by using the SWIR CAK of the GOSAT data nearest to the aircraft site from among all GOSAT data obtained within $\pm 10^\circ$ latitude–longitude boxes centered at the observation site on the same day. XCH₄ calculated using Eq. (2) with aircraft-based data weighted with the chosen GOSAT SWIR CAK is denoted as “aircraft-based XCH₄ with CAK”, and XCH₄ calculated using Eq. (3) with aircraft-based data without applying GOSAT CAK is denoted as “aircraft-based XCH₄ without CAK”.

Before examining the impact of GOSAT CAK on aircraft-based XCH₄, we show examples of vertical profiles of CH₄ concentrations and CAK over two sites (Fig. 6). At SGP on 1 September 2009, CH₄ concentrations measured by aircraft were high in the lower troposphere and then remained constant with height in the middle troposphere, similar to the GOSAT a priori profile (Fig. 6a). CAK was around unity in the troposphere. In this case, aircraft-based XCH₄ values with and without CAK were 1810.6 and 1810.0 ppb, respectively (i.e., a difference of 0.6 ppb). In the western part of Chesterfield Islands on 15 November 2009, the CH₄ profile derived from aircraft measurements, observed by a HIPPO mission, and the corrected HALOE data were almost coincident with the GOSAT a priori data (Fig. 6b). Here, CAK was larger than 0.9 in the troposphere, and the difference between aircraft-based XCH₄ with and without CAK was 0.4 ppb.

Over SGP from June 2009 to July 2010, the difference between XCH₄ with and without CAK was less than about ± 3 ppb in most cases, and the average of all differences (aircraft-based XCH₄ with CAK minus aircraft-based XCH₄ without CAK) at SGP was -0.6 ppb (Fig. 7a and Table 4). At LEF during the same period, the differences were less than about ± 6 ppb (Fig. 7b and Table 4). At all sites, the absolute value of the difference between aircraft-based XCH₄ with CAK and without CAK was estimated to be less than

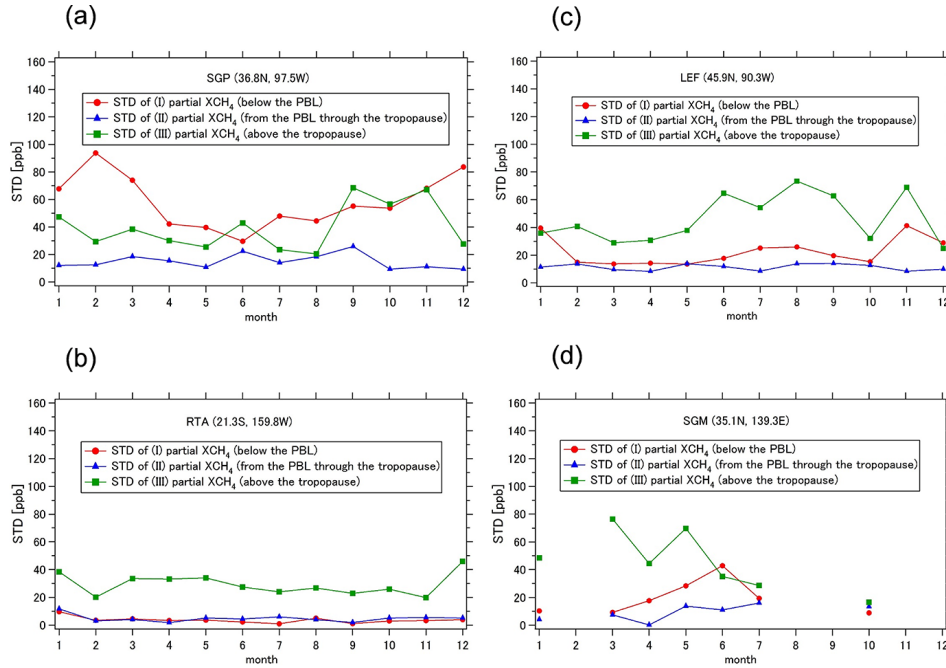


Figure 5. Monthly time series of the uncertainty of partial XCH₄ at (a) the Southern Great Plains (SGP), (b) Rarotonga (RTA), (c) Park Falls (LEF), and (d) Sagami Bay (SGM). Red circles, blue triangles, and green squares are monthly σ_{pbl} , σ_{trp} , and σ_{str} , respectively.

9 ppb at maximum, and -0.5 ppb on average with a standard deviation of 2.4 ppb (Table 4). Therefore, we concluded that the application of GOSAT SWIR CAK had only a minor effect on the aircraft-based XCH₄ calculations.

3.2 Impact of the vertical coverage of aircraft measurements on the aircraft-based XCH₄ calculation

We here investigated the impact of the vertical coverage of aircraft measurements on the aircraft-based XCH₄ calculation by using the HIPPO profiles with higher altitude observation than other aircraft platforms. Specifically, we calculated the difference between “the aircraft-based XCH₄ calculated using all aircraft data (All data XCH₄)” and “the aircraft-based XCH₄ calculated using aircraft data over a limited altitude range about 0.5–7 km (Limited data XCH₄)”. The former profile is indicated by blue solid with open circles, dashed, and dash-dotted lines in Fig. 8 (an example for HPA). The latter profile is the same as the former profile except for the altitude of 7–12.7 km, which is shown by the red line in Fig. 8. “All data XCH₄” was 1763.4 ppb and “Limited data XCH₄” was 1761.6 ppb, and the difference at HPA was as small as 1.8 ppb. The average of “All data XCH₄ minus Limited data XCH₄” calculated from all HIPPO profiles was as small as 0.4 ppb with a standard deviation of 2.2 ppb ($n = 6$).

3.3 Comparison between GOSAT XCH₄ and aircraft-based XCH₄

3.3.1 Temporally matched data

We compared aircraft-based XCH₄ calculated with CAK at each observation site with GOSAT data observed within $\pm 2^\circ$ or $\pm 5^\circ$ latitude-longitude boxes centered at each site (Fig. 9, Table 5). Within the $\pm 2^\circ$ boxes, there were a total of 43 observations over land and 3 over ocean, whereas, within the $\pm 5^\circ$ boxes, there were a total of 102 observations over land and 10 over ocean. Over the ocean, the mean bias of the GOSAT XCH₄ data relative to aircraft measurements was 4.1 ppb ($SD = 9.4$ ppb) and 6.5 ppb ($SD = 8.8$ ppb) within the $\pm 2^\circ$ and $\pm 5^\circ$ boxes, respectively. In Fig. 9, the regression lines are shown only when the regressions are statistically significant at the 99 % level. The correlation coefficients were 0.90 and 0.93 within the $\pm 2^\circ$ and $\pm 5^\circ$ boxes, respectively, though there were few samples over ocean. Over land, the mean bias of GOSAT SWIR XCH₄ relative to aircraft measurements was 1.5 ppb ($SD = 14.9$ ppb) and 2.0 ppb ($SD = 16.0$ ppb) within the $\pm 2^\circ$ and $\pm 5^\circ$ boxes, respectively, with correlation coefficients of 0.61 and 0.64, respectively, which were significant at the 99 % level.

3.3.2 Temporally interpolated aircraft-based XCH₄ data

As explained in Sect. 2.3, at some observation sites there were no flight data on the GOSAT overpass day, so it was

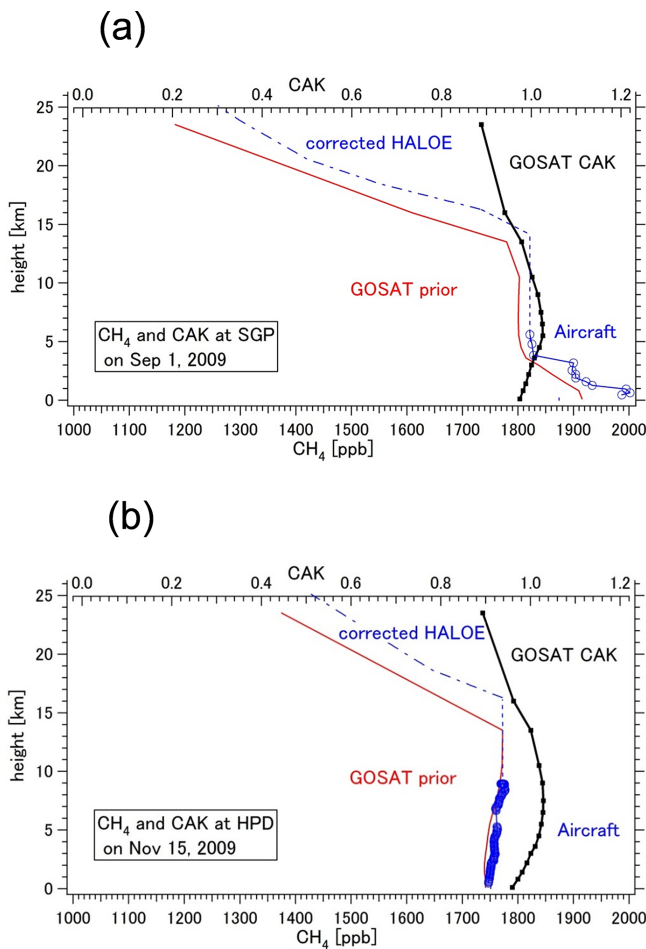


Figure 6. Vertical profiles of CH₄ and GOSAT SWIR CAK over (a) the Southern Great Plains (SGP) on 1 September 2009 and over (b) the western part of Chesterfield Islands (HPD) on 15 November 2009. The blue circles represent aircraft measurements and are connected with solid lines. The dash-dotted lines represent profiles above the tropopause based on HALOE data corrected by ACE-FTS data, and the dashed lines show where the CH₄ profiles were assumed. The red lines represent the GOSAT a priori profiles, and the black lines show GOSAT CAK.

not possible to compare GOSAT products with temporally matched aircraft measurement data. However, it was possible to obtain matched data at all observation sites by temporal interpolation of aircraft-based XCH₄ using a curve-fitting method (used for the calculation of uncertainty in Sect. 2.2.6). We fit Eq. (4) to aircraft-based XCH₄ data in the same manner as Miyamoto et al. (2013) and Inoue et al. (2013) did for XCO₂. In other words, we used curve fitting to obtain time series of aircraft-based XCH₄ without CAK after 2007, and then compared the interpolated aircraft-based XCH₄ values for the GOSAT overpass time with GOSAT XCH₄ data observed within $\pm 2^\circ$ and $\pm 5^\circ$ latitude-longitude boxes centered at the respective sites. Here, the XCH₄ data obtained by the HIPPO missions and the NIES-JAXA

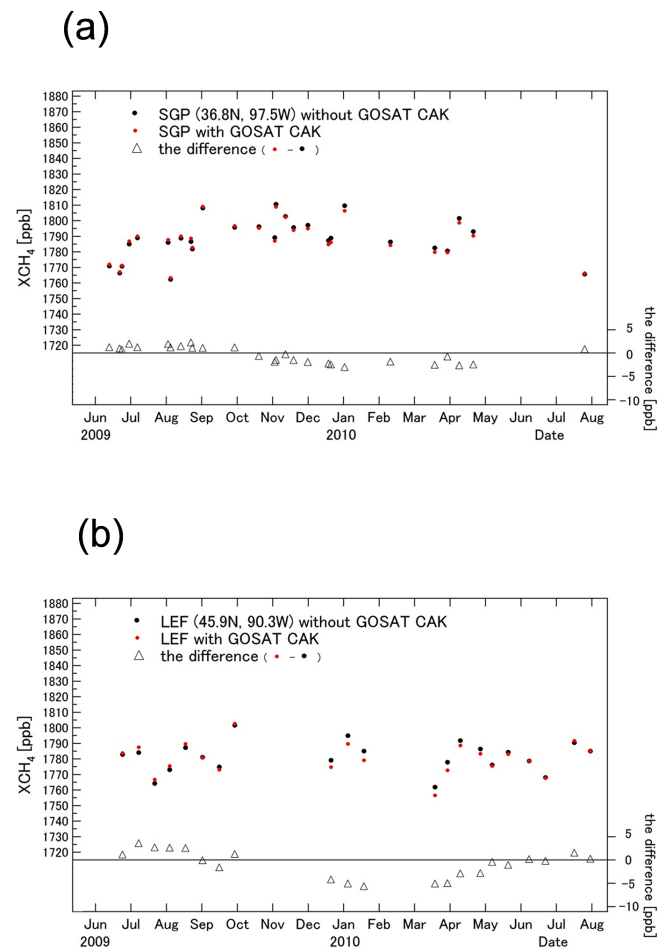


Figure 7. Temporal variations of XCH₄ with and without CAK at (a) the Southern Great Plains (SGP) and (b) Park Falls (LEF). Red and black dots indicate XCH₄ with and without the application of CAK, respectively, and the triangles show their differences.

campaign were not used for comparison of GOSAT products because it was almost impossible to obtain enough data in the same locations. In Fig. 10, we compare data within the $\pm 5^\circ$ boxes centered at SGP and Yakutsk (YAK). At SGP, aircraft-based XCH₄ varied seasonally with an amplitude of about 15 ppb, and the average growth rate of XCH₄ over the observation period (2007–2011) was 0.3 ppb month⁻¹. The average difference between GOSAT XCH₄ over land within $\pm 5^\circ$ of the site and aircraft-based XCH₄ was -8.4 ppb (SD = 16.0 ppb) at SGP and -0.2 ppb (SD = 14.5 ppb) at YAK. The correlation coefficients between the two data sets were 0.22 and 0.20 at SGP and YAK, respectively.

We next compared GOSAT SWIR XCH₄ with estimated aircraft-based XCH₄ values at the GOSAT overpass time, obtained by curve fitting and temporal interpolation, at all observation sites (Fig. 11). Over land, the mean bias of GOSAT XCH₄ was 1.0 ppb (1.5 ppb) with a standard deviation of 14.1 ppb (15.3 ppb) within the $\pm 2^\circ$ ($\pm 5^\circ$) boxes. In contrast, over ocean, the GOSAT bias was 7.1 ppb (8.4 ppb) with

Table 4. Differences between aircraft-based XCH₄ with and without application of GOSAT CAK (aircraft-based XCH₄ with CAK minus aircraft-based XCH₄ without CAK) at each site.

Site	Number	Average [ppb]	SD [ppb]	Maximum [ppb]	Minimum [ppb]
PFA	0	–	–	–	–
BRM	2	−0.5	0.9	0.2	−1.1
ESP	0	–	–	–	–
DND	8	−0.5	2.2	2.3	−3.5
LEF	21	−1.1	2.9	3.4	−5.9
NHA	19	0.0	2.8	4.3	−3.5
WBI	12	−1.8	2.1	1.9	−4.2
THD	4	0.3	2.4	2.3	−3.0
BNE	5	−1.7	2.0	1.3	−3.4
CAR	20	−3.5	2.7	−0.3	−8.9
HIL	18	−0.4	2.0	2.3	−3.6
AAO	29	1.6	1.1	3.5	−0.8
CMA	1	−2.0	–	−2.0	−2.0
SCA	11	−0.1	0.9	1.7	−0.8
TGC	7	0.1	1.6	2.4	−2.4
RTA	5	0.0	0.7	0.8	−0.9
SGP	27	−0.6	1.7	2.0	−3.2
YAK	5	0.3	0.9	1.3	−0.6
SUR	0	–	–	–	–
NOV	0	–	–	–	–
SGM	5	1.3	0.4	1.6	0.7
HPA	1	−4.1	–	−4.1	−4.1
HPB	1	0.2	–	0.2	0.2
HPC	1	1.1	–	1.1	1.1
HPD	1	0.4	–	0.4	0.4
HPE	1	−0.9	–	−0.9	−0.9
HPF	1	0.3	–	0.3	0.3
TKB	3	−1.6	0.0	−1.6	−1.7
All data	208	−0.5	2.4	4.3	−8.9

a standard deviation of 12.3 ppb (14.0 ppb) within the $\pm 2^\circ$ ($\pm 5^\circ$) boxes. The correlations between GOSAT XCH₄ and aircraft-based XCH₄ were high over both land and ocean regions: over land, the correlation coefficient was 0.56 (0.50), with significance at the 99 % level, and over ocean, it was 0.88 (0.85), with significance at the 99 % level, within the $\pm 2^\circ$ ($\pm 5^\circ$) boxes.

Finally, we compared the results obtained by direct comparison of spatiotemporally matched data with those obtained using data temporally interpolated by curve fitting (Table 6). Over land, the average difference between GOSAT data and aircraft-based data was 1–2 ppb (SD = 14–16 ppb) with both approaches. In contrast, over ocean, the average difference was 4–8 ppb (SD = 8–14 ppb). The curve-fitting method is useful for increasing the correlative data.

3.3.3 Comparison of validation results between aircraft-based data and ground-based FTS data

Finally, we compared XCH₄ validation results derived from aircraft measurements with those from ground-based FTS

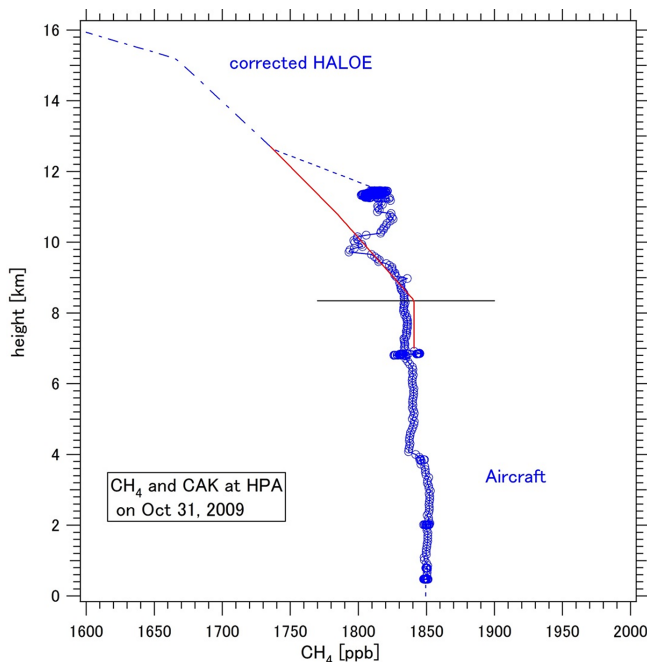


Figure 8. Vertical profiles of CH₄ over the northern part of Great Falls, Montana, obtained by the HIPPO mission (HPA) on 31 October 2009. The black horizontal line shows the tropopause. The blue dash-dotted line indicates profile by ACE/corrected HALOE (in this case, corrected HALOE), and blue dashed lines indicate the profile assumed by linear interpolation or extrapolation. The blue solid line with blue open circles shows aircraft measurements, whereas the red line shows profile assumed when using only the aircraft measurement data over a limited altitude range below 7 km (see text).

data (TCCON data). The average difference between GOSAT XCH₄ and aircraft-based XCH₄ over land within $\pm 2^\circ$ boxes was 1.5 ppb (SD = 14.9 ppb) (direct comparison) and 1.0 ppb (SD = 14.1 ppb) (curve fitting) (Table 6). Thus, with both approaches, the bias of the GOSAT SWIR Ver. 02.00 XCH₄ product over land was markedly reduced compared with the bias of the previous version of the GOSAT product (Ver. 01.xx), in which GOSAT XCH₄ was approximately 20 ppb lower than TCCON data (GGG2009 release; Morino et al., 2011). However, the aircraft measurement results reported here are not consistent with those reported by Yoshida et al. (2013), who found that the mean bias of GOSAT SWIR Ver. 02.00 XCH₄ relative to TCCON data (GGG2012 release) was −6.1 ppb (SD = 12.3 ppb). To clarify the cause of this difference, we compared the ground-based FTS data (GGG2012 release) obtained from four TCCON sites – Park Falls, Lamont (USA), Tsukuba (Japan), and Wollongong (Australia) – with aircraft measurement data at four aircraft sites (LEF, SGP, TKB, and HPC) which were obtained within $\pm 5^\circ$ boxes of each TCCON site. TCCON data are the mean values of XCH₄ data obtained within ± 30 min of GOSAT overpass time. Figure 12 and Table 7 describe the comparisons at four sites. The results show that, on average,

Table 5. Differences between GOSAT XCH₄ and aircraft-based XCH₄ at each site. The GOSAT data were retrieved over land and ocean regions within $\pm 2^\circ$ and $\pm 5^\circ$ latitude-longitude boxes centered at each aircraft observation site.

Land	$\pm 2^\circ$			$\pm 5^\circ$		
	Site	Number	Average [ppb]	SD [ppb]	Number	Average [ppb]
DND	1	19.3	–	2	21.2	2.7
LEF	3	–1.6	7.5	8	–1.1	10.6
NHA	1	5.2	–	8	13.8	24.6
WBI	1	–4.9	–	8	1.4	13.6
THD	1	14.7	–	1	14.7	–
BNE	0	–	–	2	2.5	15.1
CAR	1	–10.1	–	9	6.3	19.3
HIL	6	2.4	16.2	10	2.6	13.9
AAO	6	–0.5	11.9	19	–1.8	14.9
SCA	4	6.4	15.1	4	7.1	14.0
TGC	1	27.5	–	4	0.6	19.2
SGP	10	–9.4	16.0	15	–6.2	15.5
YAK	3	9.2	15.2	4	3.7	16.7
SGM	2	6.5	9.7	3	2.8	9.5
HPA	0	–	–	1	–11.9	–
HPF	0	–	–	1	2.7	–
TKB	3	11.4	15.4	3	11.4	15.4
All data	43	1.5	14.9	102	2.0	16.0
Ocean	$\pm 2^\circ$			$\pm 5^\circ$		
Site	Number	Average [ppb]	SD [ppb]	Number	Average [ppb]	SD [ppb]
NHA	0	–	–	1	–5.6	–
SCA	0	–	–	2	4.4	1.1
RTA	1	14.9	–	3	16.5	6.5
HPB	1	–1.8	–	1	–1.8	–
HPC	0	–	–	1	11.4	–
HPD	0	–	–	1	3.9	–
HPE	1	–0.9	–	1	–0.9	–
All data	3	4.1	9.4	10	6.5	8.8

Table 6. Differences between GOSAT XCH₄ and aircraft-based XCH₄ for all sites from the direct comparison and curve-fitting approaches.

$\pm 2^\circ$	Direct comparison			Curve-fitting method		
	Number	Average [ppb]	SD [ppb]	Number	Average [ppb]	SD [ppb]
Land	43	1.5	14.9	1543	1.0	14.1
Ocean	3	4.1	9.4	23	7.1	12.3
$\pm 5^\circ$	Direct comparison			Curve-fitting method		
	Number	Average [ppb]	SD [ppb]	Number	Average [ppb]	SD [ppb]
Land	102	2.0	16.0	8060	1.5	15.3
Ocean	10	6.5	8.8	207	8.4	14.0

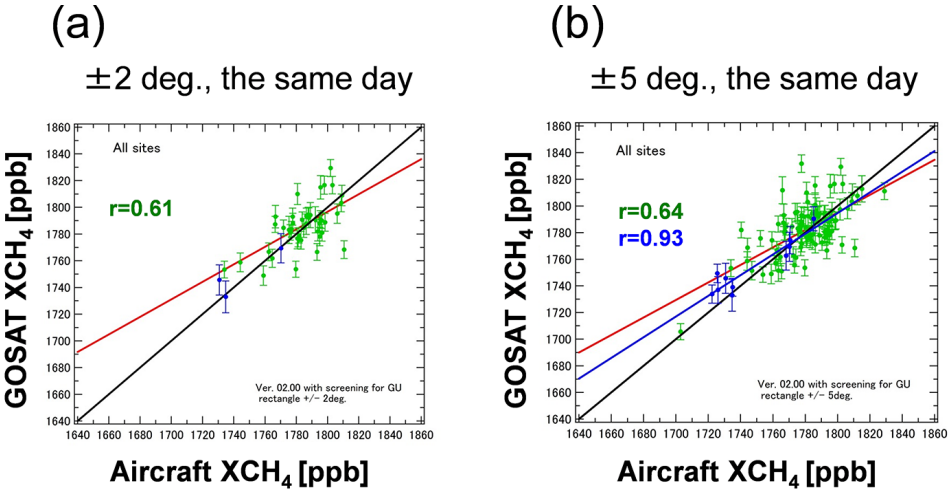


Figure 9. Scatter diagrams between GOSAT XCH₄ observed within (a) $\pm 2^\circ$ and (b) $\pm 5^\circ$ latitude–longitude boxes centered at each aircraft observation site and aircraft-based XCH₄ with the application of CAK measured on a GOSAT overpass day. Green and blue dots indicate GOSAT XCH₄ obtained over land and ocean regions, respectively. Red and blue lines denote the regression lines, statistically significant at the 99 % level, over land and ocean regions, respectively. The black lines show one-to-one correspondence.

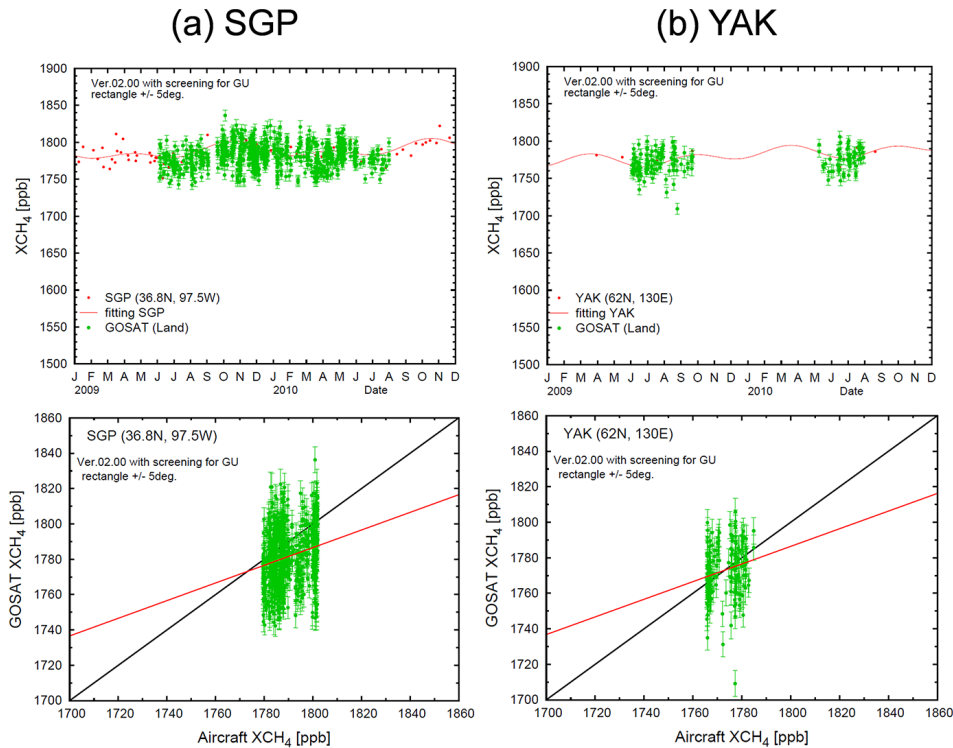


Figure 10. Temporal variations of aircraft-based XCH₄ and GOSAT XCH₄ observed within $\pm 5^\circ$ latitude–longitude boxes centered at the (a) Southern Great Plains (SGP) and (b) Yakutsk (YAK) sites (upper panels) and their scatter diagrams (bottom panels). Green dots indicate GOSAT XCH₄ data over land. Red dots and lines in the upper panels show aircraft-based XCH₄ data and curves fitted to the data, respectively. Red lines in the bottom panels are regression lines statistically significant at the 99 % level. The black lines show one-to-one correspondence.

aircraft-based XCH₄ is 8.6 ppb (SD = 10.4 ppb) smaller than TCCON XCH₄. This means that the differences between GOSAT XCH₄, TCCON XCH₄, and aircraft-based XCH₄ are consistent. The standard deviation of the GOSAT bias

over land calculated using aircraft measurements (14.9 ppb in the direct comparison) was larger than the standard deviation of the bias calculated using TCCON data (12.3 ppb). This difference may be partly because the TCCON data utilized

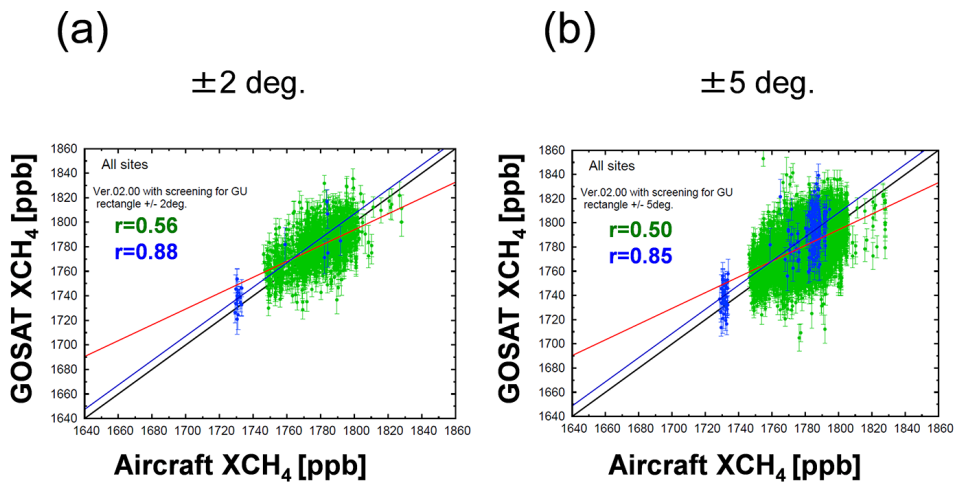


Figure 11. Scatter diagrams between GOSAT XCH₄ observed within (a) $\pm 2^\circ$ and (b) $\pm 5^\circ$ latitude–longitude boxes centered at each aircraft observation site and aircraft-based XCH₄ obtained by curve fitting at all sites. Green and blue dots indicate XCH₄ obtained over land and ocean regions, respectively. Red and blue lines denote the regression lines, statistically significant at the 99 % level, over land and ocean regions, respectively. The black lines show one-to-one correspondence.

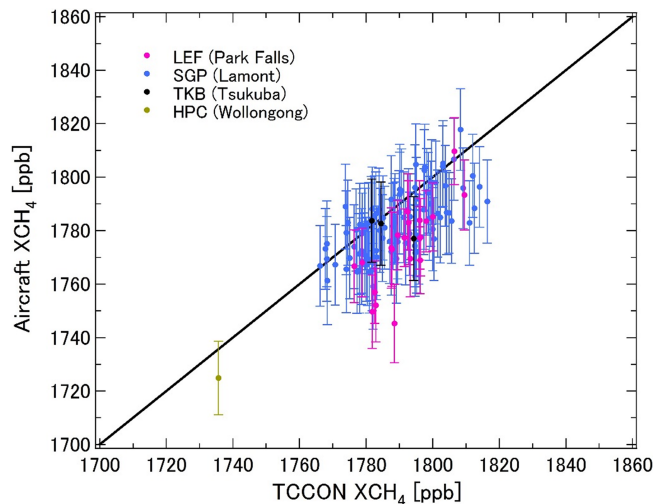


Figure 12. Scatter diagram between aircraft-based XCH₄ observed within $\pm 5^\circ$ latitude–longitude boxes centered at each TCCON site and TCCON XCH₄ (GGG2012 release) on the same day as aircraft measurement at each site. The black lines show one-to-one correspondence.

for comparison with GOSAT data were time-averaged data, whereas the aircraft measurements were obtained instantaneously at each altitude (see Inoue et al., 2013).

Some studies have compared aircraft measurements with TCCON data in terms of calibration of the TCCON FTS. Following Wunch et al. (2010) and Messerschmidt et al. (2011), Geibel et al. (2012) developed a new approach to derive a calibration factor (TCCON-to-aircraft ratio) of XCH₄ with good accuracy even for the aircraft profiles with incomplete vertical coverage. Consequently, they showed that the calibration

factor 0.978 obtained by Wunch et al. (2010) was reduced to 0.974. However, it is difficult to compare our results shown in the previous paragraph directly with those of Geibel et al. (2012), who calculated the aircraft-based XCH₄ using the GFIT a priori profile multiplied by the retrieval scaling factor for the stratospheric part of the column unlike our method. Further analyses are needed to bridge the difference between the validation results from aircraft measurements and the TCCON data.

Gavrilov et al. (2014) also compared GOSAT XCH₄ (Ver. 02.xx) with ground-based FTS data measured near St. Petersburg, Russia (59.9° N, 29.8° E), which were retrieved from mid-infrared (MIR) observations. Here we compare their result with our result at YAK located around 60° N. The average difference between GOSAT XCH₄ and aircraft-based XCH₄ within the $\pm 5^\circ$ box around YAK was 3.7 ppb (SD = 16.7 ppb) (Table 5), whereas the difference near St. Petersburg was -1.9 ppb (SD = 14.5 ppb). This difference might be due to the geographical distance separating YAK and St. Petersburg and the difference between the ground-based FTS and aircraft data as noted above.

4 Summary and conclusions

XCH₄ retrieved from GOSAT TANSO-FTS SWIR spectra (Ver. 02.00) was validated against aircraft measurement data obtained by NOAA, DOE, NIES, HIPPO, and NIES-JAXA. The stratospheric and mesospheric parts of CH₄ profiles used for calculating aircraft-based XCH₄ were obtained from ACE-FTS and HALOE climatologies. In addition, we estimated the total uncertainty of aircraft-based XCH₄ at each respective site, and screened out outlying data. Before comparing the aircraft data with GOSAT products, we

Table 7. The average, maximum, minimum, and 1 standard deviation of differences of TCCON XCH₄ (GGG2012 release) and aircraft-based XCH₄ at each observation site.

	LEF (Park Falls)	SGP (Lamont)	TKB (Tsukuba)	HPC (Wollongong)	All sites
Number	21	98	3	1	123
Average [ppb]	17.4	6.8	5.7	10.8	8.6
SD [ppb]	10.3	9.6	10.2	—	10.4
Maximum [ppb]	43.2	28.2	17.2	10.8	43.2
Minimum [ppb]	-3.2	-15.2	-2.0	10.8	-15.2

investigated differences in aircraft-based XCH₄ with and without application of GOSAT SWIR CAK and estimated them to be less than ± 9 ppb at maximum, and less than ± 1 ppb on average. Therefore, we concluded that the application of GOSAT CAK had only a minor effect on the aircraft-based XCH₄ calculation.

We compared GOSAT SWIR XCH₄ data obtained within $\pm 2^\circ$ or $\pm 5^\circ$ latitude-longitude boxes at each aircraft site with aircraft-based XCH₄ with GOSAT CAK using data measured on a GOSAT overpass day. Over land, GOSAT XCH₄ data were in good agreement with aircraft-based data, but they showed a positive bias of 1.5 ppb (2.0 ppb) with a standard deviation of 14.9 ppb (16.1 ppb) within $\pm 2^\circ$ ($\pm 5^\circ$) boxes. Over ocean, GOSAT XCH₄ data were consistent with aircraft-based data, although there were few matched data. In addition, we found the curve-fitting approach to be a useful alternative validation method. GOSAT SWIR Ver. 02.00 products over land are markedly improved compared with the previous version (Ver. 01.xx), in which XCH₄ data were lower by approximately 20 ppb than reference data. However, the differences between GOSAT XCH₄ and aircraft-based XCH₄ at individual sites were not as small as average differences among the sites. Future studies should examine differences between land and ocean regions and local differences by conducting a correlation analysis between GOSAT SWIR XCH₄ and several simultaneously retrieved parameters, including surface pressure, aerosol optical depth, and surface albedo.

Acknowledgements. DOE flights were supported by the Office of Biological and Environmental Research of the US Department of Energy under contract no. DE-AC02-05CH11231 as part of the Atmospheric Radiation Measurement Program (ARM), ARM Aerial Facility, and Terrestrial Ecosystem Science Program. We also thank the HIPPO team members for CH₄ profile data from HIPPO missions and Steven C. Wofsy at Harvard University for helpful suggestions. The HIPPO program is supported by the National Science Foundation (NSF), and its operations are managed by the Earth Observing Laboratory (EOL) of the National Center for Atmospheric Research (NCAR). We also acknowledge the Canadian Space Agency (CSA), which provides most funding support for ACE. We are grateful to the HALOE team for publishing their data for scientific use. TCCON data were obtained from the TCCON

Data Archive, operated by the California Institute of Technology (<http://tccn.ipac.caltech.edu/>). US support for TCCON retrieval software and the development of these data comes from NASA's Carbon Cycle Science Program and NASA's OCO-2 project. We are grateful to the DOE ARM program for technical support in Lamont and Jeff Ayers for technical support in Park Falls. This research was supported in part by the Environment Research and Technology Development Fund (2A-1102) of the Ministry of the Environment, Japan.

Edited by: H. Worden

References

- Andrews, A. E., Boering, K. A., Daube, B. C., Wofsy, S. C., Loewenstein, M., Jost, H., Podolske, J. R., Webster, C. R., Herman, R. L., Scott, D. C., Flesch, G. J., Moyer, E. J., Elkins, J. W., Dutton, G. S., Hurst, D. F., Moore, F. L., Ray, E. A., Romashkin, P. A., and Strahan, S. E.: Mean ages of stratospheric air derived from in situ observations of CO₂, CH₄, and N₂O, *J. Geophys. Res.*, 106, 32295–32314, doi:10.1029/2001JD000465, 2001.
- Aoki, S., Nakazawa, T., Murayama, S., and Kawaguchi, S.: Measurements of atmospheric methane at the Japanese Antarctic Station, Syowa, *Tellus B.*, 44, 273–281, doi:10.1034/j.1600-0889.1992.t01-3-00005.x, 1992.
- Araki, M., Morino, I., Machida, T., Sawa, Y., Matsueda, H., Ohyama, H., Yokota, T., and Uchino, O.: CO₂ column-averaged volume mixing ratio derived over Tsukuba from measurements by commercial airlines, *Atmos. Chem. Phys.*, 10, 7659–7667, doi:10.5194/acp-10-7659-2010, 2010.
- Aumann, H. H., Chahine, M. T., Gautier, C., Goldberg, M. D., Kalnay, E., McMillin, L. M., Revercomb, H., Rosenkranz, P. W., Smith, W. L., Staelin, D. H., Strow, L. L., and Susskind, J.: AIRS/AMSU/HSB on the Aqua mission: design, science objectives, data products, and processing systems, *IEEE Trans. Geosci. Remote Sens.*, 41, 253–264, doi:10.1109/TGRS.2002.808356, 2003.
- Bergamaschi, P., Frankenberg, C., Meirink, J. F., Krol, M., Dentener, F., Wagner, T., Platt, U., Kaplan, J. O., Körner, S., Heimann, M., Dlugokencky, E. J., and Goede, A.: Satellite chartography of atmospheric methane from SCIAMACHY on board ENVISAT: 2. Evaluation based on inverse model simulations, *J. Geophys. Res.*, 112, D02304, doi:10.1029/2006JD007268, 2007.
- Bergamaschi, P., Frankenberg, C., Meirink, J. F., Krol, M., Viliani, G. M., Houweling, S., Dentener, F., Dlugokencky, E. J.,

- Miller, J. B., Gatti, L. V., Engel, A., and Levin, I.: Inverse modeling of global and regional CH₄ emissions using SCIAMACHY satellite retrievals, *J. Geophys. Res.*, 114, D22301, doi:10.1029/2009JD012287, 2009.
- Bernath, P. F., McElroy, C. T., Abrams, M. C., Boone, C. D., Butler, M., Camy-Peyret, C., Carleer, M., Clerbaux, C., Coheur, P.-F., Colin, R., DeCola, P., De Mazière, M., Drummond, J. R., Dufour, D., Evans, W. F. J., Fast, H., Fussen, D., Gilbert, K., Jennings, D. E., Llewellyn, E. J., Lowe, R. P., Mahieu, E., McConnell, J. C., McHugh, M., McLeod, S. D., Michaud, R., Midwinter, C., Nasar, R., Nichitiu, F., Nowlan, C., Rinsland, C. P., Rochon, Y. J., Rowlands, N., Semeniuk, K., Simon, P., Skelton, R., Sloan, J. J., Soucy, M.-A., Strong, K., Tremblay, P., Turnbull, D., Walker, K. A., Walkty, I., Wardle, D. A., Wehrle, V., Zander, R., and Zou, J.: Atmospheric Chemistry Experiment (ACE): Mission overview, *Geophys. Res. Lett.*, 32, L15S01, doi:10.1029/2005GL022386, 2005.
- Biraud, S. C., Torn, M. S., Smith, J. R., Sweeney, C., Riley, W. J., and Tans, P. P.: A multi-year record of airborne CO₂ observations in the US Southern Great Plains, *Atmos. Meas. Tech.*, 6, 751–763, doi:10.5194/amt-6-751-2013, 2013.
- Blake, D. and Rowland, F. S.: Continuing worldwide increase in tropospheric methane, 1978 to 1987, *Science*, 239, 1129–1131, 1988.
- Cavanagh, L. A., Schadt, C. F., and Robinson, E.: Atmospheric hydrocarbon and carbon monoxide measurements at Point Barrow, Alaska, *Environ. Sci. Technol.*, 3, 251–257, 1969.
- Clerbaux, C., Hadji-Lazaro, J., Turquety, S., Mégie, G., and Coheur, P.-F.: Trace gas measurements from infrared satellite for chemistry and climate applications, *Atmos. Chem. Phys.*, 3, 1495–1508, doi:10.5194/acp-3-1495-2003, 2003.
- Crevoisier, C., Nobileau, D., Fiore, A. M., Armante, R., Chédin, A., and Scott, N. A.: Tropospheric methane in the tropics – first year from IASI hyperspectral infrared observations, *Atmos. Chem. Phys.*, 9, 6337–6350, doi:10.5194/acp-9-6337-2009, 2009.
- De Mazière, M., Vigouroux, C., Bernath, P. F., Baron, P., Blumenstock, T., Boone, C., Brogniez, C., Catoire, V., Coffey, M., Duchatelet, P., Griffith, D., Hannigan, J., Kasai, Y., Kramer, I., Jones, N., Mahieu, E., Manney, G. L., Piccolo, C., Randall, C., Robert, C., Senten, C., Strong, K., Taylor, J., Tétard, C., Walker, K. A., and Wood, S.: Validation of ACE-FTS v2.2 methane profiles from the upper troposphere to the lower mesosphere, *Atmos. Chem. Phys.*, 8, 2421–2435, doi:10.5194/acp-8-2421-2008, 2008.
- Dils, B., De Mazière, M., Müller, J. F., Blumenstock, T., Buchwitz, M., de Beek, R., Demoulin, P., Duchatelet, P., Fast, H., Frankenberg, C., Gloudemans, A., Griffith, D., Jones, N., Kerzenmacher, T., Kramer, I., Mahieu, E., Mellqvist, J., Mittermeier, R. L., Notholt, J., Rinsland, C. P., Schrijver, H., Smale, D., Strandberg, A., Straume, A. G., Stremme, W., Strong, K., Sussmann, R., Taylor, J., van den Broek, M., Velasco, V., Wagner, T., Warneke, T., Wiacek, A., and Wood, S.: Comparisons between SCIAMACHY and ground-based FTIR data for total columns of CO, CH₄, CO₂ and N₂O, *Atmos. Chem. Phys.*, 6, 1953–1976, doi:10.5194/acp-6-1953-2006, 2006.
- DLugokenky, E. J., Steele, L. P., Lang, P. M., and Masarie, K. A.: The growth rate and distribution of atmospheric methane, *J. Geophys. Res.*, 99, 17021–17043, doi:10.1029/94JD01245, 1994.
- Fleming, E. L., Chandra, S., Barnett, J. J., and Corney, M.: Zonal mean temperature, pressure, zonal wind and geopotential height as functions of latitude, COSPAR International Reference Atmosphere: 1986, Part II: Middle Atmosphere Models, *Adv. Space Res.*, 10, 11–59, doi:10.1016/0273-1177(90)90386-E, 1990.
- Fraser, A., Palmer, P. I., Feng, L., Boesch, H., Cogan, A., Parker, R., Dlugokencky, E. J., Fraser, P. J., Krummel, P. B., Langenfelds, R. L., O'Doherty, S., Prinn, R. G., Steele, L. P., van der Schoot, M., and Weiss, R. F.: Estimating regional methane surface fluxes: the relative importance of surface and GOSAT mole fraction measurements, *Atmos. Chem. Phys.*, 13, 5697–5713, doi:10.5194/acp-13-5697-2013, 2013.
- Fraser, P. J., Khalil, M. A. K., Rasmussen, R. A., and Crawford, A. J.: Trends of atmospheric methane in the southern hemisphere, *Geophys. Res. Lett.*, 8, 1063–1066, doi:10.1029/GL008i010p01063, 1981.
- Gavrilov, N. M., Makarova, M. V., Poberovskii, A. V., and Timofeyev, Yu. M.: Comparisons of CH₄ ground-based FTIR measurements near Saint Petersburg with GOSAT observations, *Atmos. Meas. Tech.*, 7, 1003–1010, doi:10.5194/amt-7-1003-2014, 2014.
- Geibel, M. C., Messerschmidt, J., Gerbig, C., Blumenstock, T., Chen, H., Hase, F., Kolle, O., Lavrič, J. V., Notholt, J., Palm, M., Rettinger, M., Schmidt, M., Sussmann, R., Warneke, T., and Feist, D. G.: Calibration of column-averaged CH₄ over European TCCON FTS sites with airborne in-situ measurements, *Atmos. Chem. Phys.*, 12, 8763–8775, doi:10.5194/acp-12-8763-2012, 2012.
- Groß, J.-U. and Russell, J. M.: Technical note: A stratospheric climatology for O₃, H₂O, CH₄, NO_x, HCl and HF derived from HALOE measurements, *Atmos. Chem. Phys.*, 5, 2797–2807, doi:10.5194/acp-5-2797-2005, 2005.
- Inoue, H. Y. and Matsueda, H.: Variations in atmospheric CO₂ at the Meteorological Research Institute, Tsukuba, Japan, *J. Atmos. Chem.*, 23, 137–161, 1996.
- Inoue, H. Y. and Matsueda, H.: Measurements of atmospheric CO₂ from a meteorological tower in Tsukuba, Japan, *Tellus B*, 53, 205–219, doi:10.1034/j.1600-0889.2001.01163.x, 2001.
- Inoue, M., Morino, I., Uchino, O., Miyamoto, Y., Yoshida, Y., Yokota, T., Machida, T., Sawa, Y., Matsueda, H., Sweeney, C., Tans, P. P., Andrews, A. E., Biraud, S. C., Tanaka, T., Kawakami, S., and Patra, P. K.: Validation of XCO₂ derived from SWIR spectra of GOSAT TANSO-FTS with aircraft measurement data, *Atmos. Chem. Phys.*, 13, 9771–9788, doi:10.5194/acp-13-9771-2013, 2013.
- Jones, A., Walker, K. A., Jin, J. J., Taylor, J. R., Boone, C. D., Bernath, P. F., Brohede, S., Manney, G. L., McLeod, S., Hughes, R., and Daffer, W. H.: Technical Note: A trace gas climatology derived from the Atmospheric Chemistry Experiment Fourier Transform Spectrometer (ACE-FTS) data set, *Atmos. Chem. Phys.*, 12, 5207–5220, doi:10.5194/acp-12-5207-2012, 2012.
- Kort, E. A., Wofsy, S. C., Daube, B. C., Diao, M., Elkins, J. W., Gao, R. S., Hintsa, E. J., Hurst, D. F., Jimenez, R., Moore, F. L., Spackman, J. R., and Zondlo, M. A.: Atmospheric observations of Arctic Ocean methane emissions up to 82° north, *Nat. Geosci.*, 5, 318–321, doi:10.1038/ngeo1452, 2012.
- Kuze, A., Suto, H., Nakajima, M., and Hamazaki, T.: Thermal and near infrared sensor for carbon observation Fourier-transform spectrometer on the Greenhouse Gases Observing Satellite for

- greenhouse gases monitoring, *Appl. Optics*, 48, 6716–6733 doi:10.1364/AO.48.006716, 2009.
- Machida, T., Nakazawa, T., Ishidoya, S., Maksyutov, S., Tohjima, Y., Takahashi, Y., Watai, T., Vinnichenko, N., Panchenko, M., Arshinov, M., Fedoseev, N., and Inoue, G.: Temporal and spatial variations of atmospheric CO₂ mixing ratio over Siberia, Ext. Abstr. 6th International CO₂ Conf., 1–5 October, Sendai, Japan, 2001.
- Machida, T., Matsueda, H., Sawa, Y., Nakagawa, Y., Hirotani, K., Kondo, N., Goto, K., Nakazawa, T., Ishikawa, K., and Ogawa, T.: Worldwide measurements of atmospheric CO₂ and other trace gas species using commercial airlines, *J. Atmos. Oceanic Technol.*, 25, 1744–1754, doi:10.1175/2008JTECHA1082.1, 2008.
- Maksyutov, S., Patra, P. K., Onishi, R., Saeki, T., and Nakazawa, T.: NIES/FRCGC global atmospheric tracer transport model: Description, validation, and surface sources and sinks inversion, *J. Earth Sim.*, 9, 3–18, 2008.
- Matsueda, H. and Inoue, H. Y.: Measurements of atmospheric CO₂ and CH₄ using a commercial airliner from 1993 to 1994, *Atmos. Environ.*, 30, 1647–1655, 1996.
- Meirink, J. F., Bergamaschi, P., Frankenberg, C., d'Amelio, M. T. S., Dlugokencky, E. J., Gatti, L. V., Houweling, S., Miller, J. B., Röckmann, T., Villani, M. G., and Krol, M. C.: Four-dimensional variational data assimilation for inverse modeling of atmospheric methane emissions: Analysis of SCIAMACHY observations, *J. Geophys. Res.*, 113, D17301, doi:10.1029/2007JD009740, 2008.
- Messerschmidt, J., Geibel, M. C., Blumenstock, T., Chen, H., Deutscher, N. M., Engel, A., Feist, D. G., Gerbig, C., Gisi, M., Hase, F., Katrynski, K., Kolle, O., Lavrič, J. V., Notholt, J., Palm, M., Ramonet, M., Rettinger, M., Schmidt, M., Sussmann, R., Toon, G. C., Truong, F., Warneke, T., Wennberg, P. O., Wunch, D., and Xueref-Remy, I.: Calibration of TCCON column-averaged CO₂: the first aircraft campaign over European TCCON sites, *Atmos. Chem. Phys.*, 11, 10765–10777, doi:10.5194/acp-11-10765-2011, 2011.
- Miyamoto, Y., Inoue, M., Morino, I., Uchino, O., Yokota, T., Machida, T., Sawa, Y., Matsueda, H., Sweeney, C., Tans, P. P., Andrews, A. E., Biraud, S. C., and Patra, P. K.: Atmospheric column-averaged mole fractions of carbon dioxide at 53 aircraft measurement sites, *Atmos. Chem. Phys.*, 13, 5265–5275, doi:10.5194/acp-13-5265-2013, 2013.
- Morino, I., Uchino, O., Inoue, M., Yoshida, Y., Yokota, T., Wennberg, P. O., Toon, G. C., Wunch, D., Roehl, C. M., Notholt, J., Warneke, T., Messerschmidt, J., Griffith D. W. T., Deutscher, N. M., Sherlock, V., Connor, B., Robinson, J., Sussmann, R., and Rettinger, M.: Preliminary validation of column-averaged volume mixing ratios of carbon dioxide and methane retrieved from GOSAT short-wavelength infrared spectra, *Atmos. Meas. Tech.*, 4, 1061–1076, doi:10.5194/amt-4-1061-2011, 2011.
- Pan, L. L. and Munchak, L. A.: Relationship of cloud top to the tropopause and jet structure from CALIPSO data, *J. Geophys. Res.*, 116, D12201, doi:10.1029/2010JD015462, 2011.
- Park, J. H., Russell III, J. M., Gordley, L. L., Drayson, S. R., Benner, D. C., McInerney, J. M., Gunson, M. R., Toon, G. C., Sen, B., Blavier, J-F., Webster, C. R., Zipf, E. C., Erdman, P., Schmidt, U., and Schiller, C.: Validation of Halogen Occultation Experiment CH₄ measurements from the UARS, *J. Geophys. Res.*, 101, D6, 10183–10203, doi:10.1029/95JD02736, 1996.
- Parker, R., Boesch, H., Cogan, A., Fraser, A., Feng, L., Palmer, P. I., Messerschmidt, J., Deutscher, N., Griffith, D. W. T., Notholt, J., Wennberg, P. O., and Wunch, D.: Methane observations from the Greenhouse Gases Observing SATellite: Comparison to ground-based TCCON data and model calculations, *Geophys. Res. Lett.*, 38, L15807, doi:10.1029/2011GL047871, 2011.
- Saeki, T., Saito, R., Belikov, D., and Maksyutov, S.: Global high-resolution simulations of CO₂ and CH₄ using a NIES transport model to produce a priori concentrations for use in satellite data retrievals, *Geosci. Model Dev.*, 6, 81–100, doi:10.5194/gmd-6-81-2013, 2013.
- Saitoh, N., Touno, M., Hayashida, S., Imasu, R., Shiomi, K., Yokota, T., Yoshida, Y., Machida, T., Matsueda, H., and Sawa, Y.: Comparisons between XCH₄ from GOSAT Shortwave and Thermal Infrared Spectra and Aircraft CH₄ Measurement over Guam, *Sci. Online Lett. Atmos. (SOLA)*, 8, 145–149, doi:10.2151/sola.2012-036, 2012.
- Sasakawa, M., Shimoyama, K., Machida, T., Tsuda, N., Suto, H., Arshinov, M., Davydov, D., Fofonov, A., Krasnov, O., Saeki, T., Koyama, Y., and Maksyutov, S.: Continuous measurements of methane from a tower network over Siberia, *Tellus, Ser. B*, 62, 403–416, doi:10.1111/j.1600-0889.2010.00494.x, 2010.
- Schepers, D., Guerlet, S., Butz, A., Landgraf, J., Frankenberg, C., Hasekamp, O., Blavier, J.-F., Deutscher, N. M., Griffith, D. W. T., Hase, F., Kyrö, E., Morino, I., Sherlock, V., Sussmann, R., and Aben, I.: Methane retrievals from Greenhouse Gases Observing Satellite (GOSAT) shortwave infrared measurements: Performance comparison of proxy and physics retrieval algorithms, *J. Geophys. Res.*, 117, D10307, doi:10.1029/2012JD017549, 2012.
- Schneising, O., Buchwitz, M., Burrows, J. P., Bovensmann, H., Bergamaschi, P., and Peters, W.: Three years of greenhouse gas column-averaged dry air mole fractions retrieved from satellite – Part 2: Methane, *Atmos. Chem. Phys.*, 9, 443–465, doi:10.5194/acp-9-443-2009, 2009.
- Schneising, O., Bergamaschi, P., Bovensmann, H., Buchwitz, M., Burrows, J. P., Deutscher, N. M., Griffith, D. W. T., Heymann, J., Macatangay, R., Messerschmidt, J., Notholt, J., Rettinger, M., Reuter, M., Sussmann, R., Velasco, V. A., Warneke, T., Wennberg, P. O., and Wunch, D.: Atmospheric greenhouse gases retrieved from SCIAMACHY: comparison to ground-based FTS measurements and model results, *Atmos. Chem. Phys.*, 12, 1527–1540, doi:10.5194/acp-12-1527-2012, 2012.
- Steele, L., Fraser, P., Rasmussen, R., Khalil, M., Conway, T., Crawford, A., Gammon, R., Masarie, K., and Thoning, K.: The global distribution of methane in the troposphere, *J. Atmos. Chem.*, 5, 125–171, 1987.
- Tanaka, T., Miyamoto, Y., Morino, I., Machida, T., Nagahama, T., Sawa, Y., Matsueda, H., Wunch, D., Kawakami, S., and Uchino, O.: Aircraft measurements of carbon dioxide and methane for the calibration of ground-based high-resolution Fourier Transform Spectrometers and a comparison to GOSAT data measured over Tsukuba and Moshiri, *Atmos. Meas. Tech.*, 5, 2003–2012, doi:10.5194/amt-5-2003-2012, 2012.
- Terao, Y., Mukai, H., Nojiri, Y., Machida, T., Tohjima, Y., Saeki, T., and Maksyutov, S.: Interannual variability and trends in atmospheric methane over the western Pacific from 1994 to 2010, *J. Geophys. Res.*, 116, D14303, doi:10.1029/2010JD015467, 2011.
- Tohjima, Y., Wakita, H., Maksyutov, S., Machida, T., Inoue, G., Vinnichenko, N., and Khattatov, V.: Distribution of tropospheric

- methane over Siberia in July 1993, *J. Geophys. Res.*, 102, 25371–25382, doi:10.1029/97JD02244, 1997.
- Tohjima, Y., Machida, T., Utiyama, M., Katsumoto, M., Fujinuma, Y., and Maksyutov, S.: Analysis and presentation of in situ atmospheric methane measurements from Cape Ochi-ishi and Hateruma Island, *J. Geophys. Res.*, 107, 4148, doi:10.1029/2001JD001003, 2002.
- Wada, A., Matsueda, H., Sawa, Y., Tsuboi, K., and Okubo, S.: Seasonal variation of enhancement ratios of trace gases observed over 10 years in the western North Pacific, *Atmos. Environ.*, 45, 2129–2137, doi:10.1016/j.atmosenv.2011.01.043, 2011.
- Wecht, K. J., Jacob, D. J., Wofsy, S. C., Kort, E. A., Worden, J. R., Kulawik, S. S., Henze, D. K., Kopacz, M., and Payne, V. H.: Validation of TES methane with HIPPO aircraft observations: implications for inverse modeling of methane sources, *Atmos. Chem. Phys.*, 12, 1823–1832, doi:10.5194/acp-12-1823-2012, 2012.
- Wofsy, S. C. and the HIPPO Science Team and Cooperating Modellers and Satellite Teams: HIAPER Pole-to-Pole Observations (HIPPO): fine-grained, global-scale measurements of climatically important atmospheric gases and aerosols, *Philos. T. Roy. Soc. A*, 369, 2073–2086, doi:10.1098/rsta.2010.0313, 2011.
- Wofsy, S. C., Daube, B. C., Jimenez, R., Kort, E., Pittman, J. V., Park, S., Commane, R., Xiang, B., Santoni, G., Jacob, D., Fisher, J., Pickett-Heaps, C., Wang, H., Wecht, K., Wang, Q.-Q., Stephens, B. B., Shertz, S., Watt, A. S., Romashkin, P., Campos, T., Haggerty, J., Cooper, W. A., Rogers, D., Beaton, S., Hendershot, R., Elkins, J. W., Fahey, D. W., Gao, R. S., Moore, F., Montzka, S. A., Schwarz, J. P., Perring, A. E., Hurst, D., Miller, B. R., Sweeney, C., Oltmans, S., Nance, D., Hints, E., Dutton, G., Watts, L. A., Spackman, J. R., Rosenlof, K. H., Ray, E. A., Hall, B., Zondlo, M. A., Diao, M., Keeling, R., Bent, J., Atlas, E. L., Lueb, R., and Mahoney, M. J.: HIPPO merged 10-second Meteorology, Atmospheric Chemistry, Aerosol Data (R_20121129), used data file “HIPPO_all_missions_merged_10s_20121129.tbl”, Carbon Dioxide Information Analysis Center, Oak Ridge National Laboratory, Oak Ridge, Tennessee, USA, doi:10.3334/CDIAC/hippo_010, 2012.
- Wunch, D., Toon, G. C., Wennberg, P. O., Wofsy, S. C., Stephens, B. B., Fischer, M. L., Uchino, O., Abshire, J. B., Bernath, P., Braud, S. C., Blavier, J.-F. L., Boone, C., Bowman, K. P., Browell, E. V., Campos, T., Connor, B. J., Daube, B. C., Deutscher, N. M., Diao, M., Elkins, J. W., Gerbig, C., Gottlieb, E., Griffith, D. W. T., Hurst, D. F., Jiménez, R., Keppel-Aleks, G., Kort, E. A., Macatangay, R., Machida, T., Matsueda, H., Moore, F., Morino, I., Park, S., Robinson, J., Roehl, C. M., Sawa, Y., Sherlock, V., Sweeney, C., Tanaka, T., and Zondlo, M. A.: Calibration of the Total Carbon Column Observing Network using aircraft profile data, *Atmos. Meas. Tech.*, 3, 1351–1362, doi:10.5194/amt-3-1351-2010, 2010.
- Wunch, D., Toon, G. C., Blavier, J.-F. L., Washenfelder, R. A., Notholt, J., Connor, B. J., Griffith, D. W. T., Sherlock, V., and Wennberg, P. O.: The Total Carbon Column Observing Network, *Phil. Trans. R. Soc. A*, 369, 2087–2112, doi:10.1098/rsta.2010.0240, 2011.
- Xiong, X., Barnet, C., Maddy, E., Sweeney, C., Liu, X., Zhou, L., and Goldberg, M.: Characterization and validation of methane products from the Atmospheric Infrared Sounder (AIRS), *J. Geophys. Res.*, 113, G00A01, doi:10.1029/2007JG000500, 2008.
- Yokota, T., Yoshida, Y., Eguchi, N., Ota, Y., Tanaka, T., Watanabe, H., and Maksyutov, S.: Global Concentrations of CO₂ and CH₄ Retrieved from GOSAT: First Preliminary Results, *Sci. Online Lett. Atmos. (SOLA)*, 5, 160–163, doi:10.2151/sola.2009-041, 2009.
- Yoshida, Y., Ota, Y., Eguchi, N., Kikuchi, N., Nobuta, K., Tran, H., Morino, I., and Yokota, T.: Retrieval algorithm for CO₂ and CH₄ column abundances from short-wavelength infrared spectral observations by the Greenhouse gases observing satellite, *Atmos. Meas. Tech.*, 4, 717–734, doi:10.5194/amt-4-717-2011, 2011.
- Yoshida, Y., Kikuchi, N., Morino, I., Uchino, O., Oshchepkov, S., Bril, A., Saeki, T., Schutgens, N., Toon, G. C., Wunch, D., Roehl, C. M., Wennberg, P. O., Griffith, D. W. T., Deutscher, N. M., Warneke, T., Notholt, J., Robinson, J., Sherlock, V., Connor, B., Rettinger, M., Sussmann, R., Ahonen, P., Heikkinen, P., Kyrö, E., Mendonca, J., Strong, K., Hase, F., Dohe, S., and Yokota, T.: Improvement of the retrieval algorithm for GOSAT SWIR XCO₂ and XCH₄ and their validation using TCCON data, *Atmos. Meas. Tech.*, 6, 1533–1547, doi:10.5194/amt-6-1533-2013, 2013.